ACS APPLIED MATERIALS & INTERFACES

Review

Cite This: ACS Appl. Mater. Interfaces 2020, 12, 14721−14738

www.acsami.org

Multimodal Characterization of Materials and Decontamination Processes for Chemical Warfare Protection

Amani M. Ebrahim,[†] Anna M. Plonka,[†] Yiyao Tian,[†] Sanjaya D. Senanayake,[‡] Wesley O. Gordon,[§] Alex Balboa,[§] Hui Wang,[§] Daniel L. Collins-Wildman,[∥] Craig L. Hill,[∥] Djamaladdin G. Musaev,[∥,⊥] John R. Morris,[#] Diego Troya,[#] and Anatoly I. Frenkel*[,†,‡]

[†]Department of Materials Science and Chemical Engineering, Stony Brook University, Stony Brook, New York 11794, United States

[‡]Chemistry Division, Brookhaven National Laboratory, Upton, New York 11973, United States

[§]U.S. Army Combat Capabilities Development Command Chemical Biological Center, Aberdeen Proving Ground, Maryland 21010, United States

[∥]Department of Chemistry, Emory University, Atlanta, Georgia 30322, United States

[⊥]Cherry L. Emerson Center for Scientific Computation, Emory University, Atlanta, Georgia 30322, United States

[#]Department of Chemistry, Virginia Tech, Blacksburg, Virginia 24061, United States

ABSTRACT: This Review summarizes the recent progress made in the field of chemical threat reduction by utilizing new in situ analytical techniques and combinations thereof to study multifunctional materials designed for capture and decomposition of nerve gases and their simulants. The emphasis is on the use of in situ experiments that simulate realistic operating conditions (solid−gas interface, ambient pressures and temperatures, time-resolved measurements) and advanced synchrotron methods, such as in situ X-ray absorption and scattering methods, a combination thereof with other complementary measurements (e.g., XPS, Raman, DRIFTS, NMR), and theoretical modeling. The examples presented in this Review range from studies of the adsorption and decomposition of nerve agents and their simulants on Zr-based metal organic frameworks to Nb and Zr-based polyoxometalates and metal (hydro)oxide materials. The approaches employed in these studies ultimately demonstrate how advanced synchrotron-based in situ X-ray absorption spectroscopy and diffraction can be exploited to develop an atomic- level understanding of interfacial binding and reaction of chemical warfare agents, which impacts the development of novel filtration media and other protective materials.

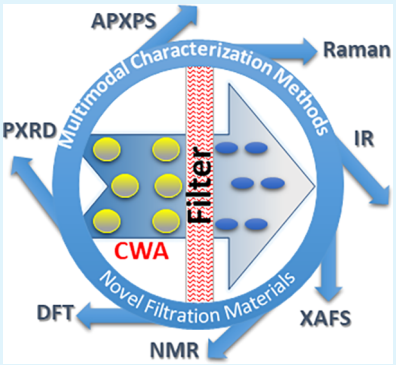

KEYWORDS: *chemical warfare agents, simulants, metal−organic frameworks, polyoxometalates, X-ray absorption fine structure spectroscopy, X-ray diffraction, in situ characterization*

1. INTRODUCTION

Ever since their inception during World War I, chemical warfare agents (CWAs) have created events of lethal catastrophic proportions and their usage remains a serious threat to civilians and military personnel.[1] The filtration and decontamination of these hazardous agents is essential to mitigate risks of exposure and to protect people in case of deliberate use. The primary treatment and management of dermal exposure to CWAs is multifaceted and involves several extensive steps. The first means of dermal exposure mitigation is through the donning of appropriate proper personal protective equipment (PPE), which includes gas masks and filters. The PPE must thus be able to capture and detoxify the released gases/vapors. To properly engineer such filtration materials, a complete understanding of how these filters interact with CWAs in realistic conditions, including the effects of surrounding gases in ambient air, must also be addressed. In addition, the development of efficient filtration media requires our understanding of not only the effects of environmental gases on the structural and electronic properties of the materials being used but also how such competing gases may be involved in the decontamination process.

A fundamental understanding of what occurs at the solid−multigas interface is of critical importance for the development of efficient air filtration technologies and decontamination materials. The sparsity of effective materials is due, in part, to the paucity of methods to study their functional mechanisms at the atomic level and in real working (operando) conditions. Because of the complexity of the interactions of CWAs with filtration materials, a multimodal approach is required to characterize the changes that occur in both the adsorbing materials and the adsorbed species in a complementary

Special Issue: Nanomaterial Development, Characterization, and Integration Strategies for Chemical Warfare Defense

Received: October 28, 2019
Accepted: December 9, 2019
Published: December 9, 2019

DOI: 10.1021/acsami.9b19494
ACS Appl. Mater. Interfaces 2020, 12, 14721−14738

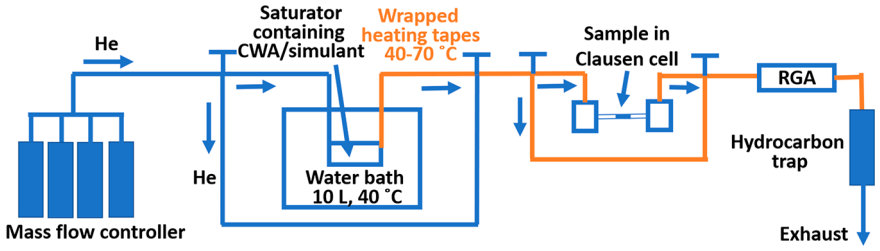

Figure 1. Schematic representing the design of agent/simulant delivery into a Clausen cell for in situ/operando studies. A mass flow controller carries a well-defined volumetric flow rate of carrier gas (helium or nitrogen) into the glass fritted microsaturator that is contained in a large water bath kept isothermally at 40 °C. The outlet of the cell is connected to PEEK lines that are heated and carry the diluted organic vapor into the powder sample housed in the Clausen cell. The outlet vapors (exhaust of the cell) flow into a residual gas analyzer (RGA) and then to a carbon trap before reaching the exhaust.

manner. Such methods have been undergoing rapid development in catalysis science in the past few years, and many examples of multimodal, operando characterization approaches have been reviewed recently.[2−5] In this Review, we summarize recent developments of multimodal, operando characterization methodologies specific to the research and development of novel multifunctional decontaminating materials.

A unique aspect of nerve agents that complicates their fundamental research is their acute toxicity. An accepted approach to study the uptake, decontamination and other chemistry of these dangerous agents is to rely on simulants that mimic their physicochemical and other properties. While the choice of a simulant for a given agent is often not straightforward, the simulants are a crucial component in CWA filtration studies because of the relative ease with which simulants can be studied at multiple characterization facilities. In addition to experimental approaches, computational methods and quantitative structure−activity relationships have provided vital information to correlate properties of the agents with their respective simulants.[6] For example, Mendonca and Snurr have screened over 100 organophosphate molecules and assessed their similarities to the real agents Soman (GD) and Sarin (GB).[6] Beyond establishing a proper simulant for agent studies, the improvement of detection methods for simulants of Sarin and Soman has also been an active area of research. Gotor et al. were successful in creating a molecular probe for the sole detection of a simulant of Sarin, diisopropylfluorophosphate (DFP), with high accuracy despite the presence of other organophosphate containing compounds.[7] In addition, the ability to detect nerve agents and sense their potency is equally important, and a recent study has shown one of the first demonstrations of a gradient sensor to detect nerve agents with a concentration as low as 20 ppb in 20 s.[8]

In addition to understanding how nerve agents interact with filtration materials in real battlefield conditions, another important field of research lies in nerve agent destruction.[9] Several routes have been adopted to convert these agents into more benign products. Decontamination of nerve agents can occur via mechanical (mixing agent under layers of soil), physical (dilution, washing, and adsorption) or chemical means (hydrolysis, elimination, or oxidation).[8,10] The underlying chemistry for the decomposition of nerve agents depends primarily on the hydrolysis of the most labile P−X bond. Several efforts have been utilized to improve the cleavage of this bond. Several methods have been previously used for the destruction of nerve agents, such as incineration, neutralization by base, oxidation by bleach and peroxides, enzyme-assisted degradation, and metal-catalyzed systems. However, almost all these routes suffer from their irreproducibility on a large scale, occur in the liquid phase, require large amounts of energy, require precise stoichiometry of base, may have short shelf lives, may have slow reaction kinetics, or do not have justifiable feasibility for working conditions.[9−11]

Just as the studies of filter−agent interaction at the solid−vapor interface are required for fundamental understanding of their mechanisms, so are the studies of the agent decontamination pathways. In addition to solid formulations that include Sandia's decontamination foam, decontamination sponges, polyurethane foams, and dry woven pads, other formulations such as EasyDECON DF200 decontamination solution are especially effective when dispersed as compressed air foam.[9]

Most adsorbents are designed to improve the capture and decontamination efficiency of CWAs and are developed to combat a specific class of chemistry prevalent in CWAs. Several porous (hydro)oxides of various metals have been used as potential decontaminating materials. A zinc, iron, and copper hydroxide prepared by a coprecipitation method converted harmful 2-chloroethyl ethyl sulfide (2-CEES), a simulant of mustard gas, into methyl chloride and ethylvinyl sulfide, a nontoxic byproduct. Metal (hydro)oxides and their composites have also shown good response to CWA uptake and decomposition at ambient conditions.[12−16] For example, titania/ceria composites were determined to be efficient in the degradation of dimethyl methylphosphonate (DMMP), a simulant of Sarin, via the surface-active sites introduced by the doping of Ti^{2+} sites into ceria. Furthermore, Janõs and coworkers indicated that the quality and type of ceria and the hydroxyl density plays an additional crucial role in the hydrolysis kinetics.[17] Iron−manganese oxide composites were found to be reactive toward Soman.[18] Polyoxometalates (POMs), a class of anionic polynuclear metal-oxo ensembles of early transition metals with pseudo-octahedral units with unique surface charge densities, have also shown promising applications in the hydrolysis of nerve agents.[19−22] Carbon-based materials, such as activated carbons, graphitic carbon, graphene oxide, single/multi-walled carbon nanotubes, and graphite oxides have also shown to capture nerve agents readily.[23−27]

Another class of material that leverages the hybrid chemistry found in oxides are metal organic frameworks (MOFs). MOFs are porous materials that can offer a novel support to disperse, anchor, and activate metal sites to yield chemistry not possible with other materials. Changes in their surface areas, pore volumes, and topology give rise to different adsorptive

DOI: 10.1021/acsami.9b19494
ACS Appl. Mater. Interfaces 2020, 12, 14721−14738

behaviors. Mixed MOFs and composite MOFs have also shown an increase in uptake and decontamination of CWAs.[28−31]

While many solid sorbent formulations have demonstrated promise for decontamination in controlled liquid phase conditions, a detailed understanding of their working mechanisms in the presence of environmental contaminants, at the battlefield-realistic solid−vapor interface, remains a challenge. Those contaminants include ambient gases, such as carbon dioxide, water vapor, nitrogen dioxide, and sulfur dioxide.[32] Further complicating informative studies of decontamination are the evident effect of temperature and the presence of UV light. The adsorption process itself is affected by moisture.[33] In short, the most insightful studies of agent decontamination and optimization of these processes need to be conducted under realistic external conditions.

2. APPROACH TO THE IMPLEMENTATION OF REALISTIC CONDITIONS BY USING IN SITU MEASUREMENTS

Several examples of correlative, multimodal investigations shown below adopt the design for agent vapor delivery into reaction cells for in situ/operando studies, developed in the U.S. Army Combat Capabilities Development Command (CCDC) Chemical Biological Center (CBC). The schematic of the setup is shown in Figure 1.

This setup enables the delivery of controlled concentrations of the agent for a real-time analysis of the filtration material's structure, surface composition, and agent uptake and decomposition. The simplicity of the design was important for its reproduction at Brookhaven National Laboratory (BNL), where a dedicated setup was built at the Structure and Dynamics of Applied Nanomaterials laboratory in the Chemistry Division. In addition, a portable setup was designed and built for operations at various X-ray absorption spectroscopy and scattering beamlines of BNL's Light Source-II (NSLS-II), Argonne National Laboratory's Advanced Photon Source (APS) and SLAC Linear Accelerator Laboratory's Stanford Synchrotron Radiation Lightsource (SSRL). These portable setups were designed for correlative studies of simulants, delivered in the same conditions as the agents, hence, enabling their direct comparison in realistic operating conditions.

In the remainder of this Review, we highlight the complementary methods and their combinations, for a comprehensive understanding of chemical transformations upon interactions of the filtration materials with the agents/simulants.

3. POWDER X-RAY DIFFRACTION

Powder X-ray diffraction (PXRD) is among the most powerful tools for materials characterization. It has rapid acquisition times, is nondestructive, is widely accessible and is relatively easy to implement without extensive sample preparation. PXRD is used to structurally characterize both organic and inorganic crystalline samples in fields as wide as material science, polymers, nanocomposites, metallurgy, environmental sciences, pharmaceuticals, geology, archeology, or forensic science.[34] The majority of powder diffraction experiments utilize a monochromatic, collimated beam of X-rays which is directed on the sample containing multiple randomly oriented crystallites and enters the crystal lattice where atoms serve as a diffraction grating. The diffraction maxima appear when a subset of crystallites is in an orientation that satisfies Bragg's law

$$\lambda = 2d_{hkl} \sin \theta_{hkl}$$

where λ is a wavelength of the incident wave, θ_{hkl} is a scattering angle, and d_{hkl} is an interplanar distance for the planes with Miller index hkl in the crystal structure of the material. On the diffraction pattern (diffractogram) the intensity of scattered X-rays is usually plotted versus 2θ angle.

In the field of CWA decontamination, PXRD is used primarily for the initial sample characterization prior to the uptake/decomposition studies. Because each crystalline solid produces a distinct diffraction pattern, in mixtures those patterns are superimposed allowing one to analyze sample purity or phase composition.[35−40] Further, the nature of the PXRD method requires crystalline materials with an extensive long-range order. On the basis of the quality of the diffractogram, we can extract information, such as crystallinity of the sample, defined as size of coherently diffracting domains, or the possible presence of defects, stacking faults or partial framework collapse. PXRD is also used to determine the thermal or chemical stability of the material[41−46] or to understand how doping or ion exchange influences the parent structure.[43,45,47−49] The analysis of diffraction peak shape can also be used to calculate the average size of crystallites[35,43,50] as a decrease in particle size leads to the broadening of diffraction peaks. Below the Scherrer limit, the mean particle size t can be estimated using Scherrer equation

$$t = \frac{K\lambda}{B \cos \theta}$$

where K corresponds to the shape factor (typically ~1), λ and θ equal the wavelength and the incident angle of the X-rays, respectively, and B is the measured full-width at half-maximum values of a diffraction peak.[51,52]

The above-mentioned aspects of PXRD analysis can be also applied to samples recovered after an adsorption process or catalytic transformation, to understand how the structure, particle size or phase composition is influenced by the reaction with the CWA or CWA simulant. Here, the diffractogram collected before the reaction is typically compared to the one collected from the recovered sample. If the patterns are a close match, it is assumed that no significant phase transformation occurred. However, partial degradation of the material may still lead to a similar enough pattern and it is advised to perform more in-depth analysis such as full profile fitting or use complementary techniques like surface area measurements or thermogravimetry to fully assess the stability of the catalyst.[42] PXRD is widely used in the field of MOFs, where the technique is applied to confirm porous framework stability both in powder[53−62] or crystallized on textile surfaces.[63,64] Material stability based on PXRD in CWA degradation reactions has also been reported for metal oxides,[65] metal/enzymatic nanoreactors,[66] and polyoxometalates, from samples collected both ex situ after the reaction[67,68] or collected in situ during a flow-reactor experiment.[21]

When the catalyst undergoes structural changes during the reaction with CWA, PXRD can be used for phase analysis of the products formed or structural refinement of the catalyst. Tian et al., reported that upon dimethyl chlorophosphate (DMCP) and Sarin exposure a dimeric Zr-containing polytungstate undergoes monomerization, making coordina-

DOI: 10.1021/acsami.9b19494
ACS Appl. Mater. Interfaces 2020, 12, 14721−14738

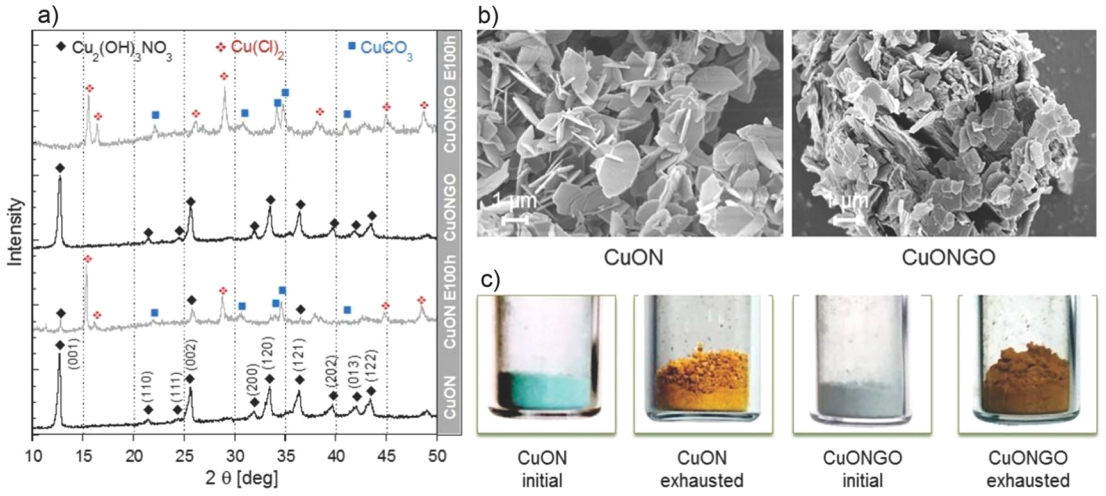

Figure 2. (a) X-ray diffraction patterns, (b) SEM images and (c) pictures of the initial and exhausted samples of copper hydroxyl nitrate (CuON) and copper hydroxyl nitrate/graphite oxide composite (CuONGO). Notice the formation of the new crystalline phases of $Cu(Cl)_2$ and $CuCO_3$ after the reaction. Reprinted with permission from ref 66. Copyright 2015 WILEY-VCH Verlag GmbH & Co. KGaA, Weinheim.

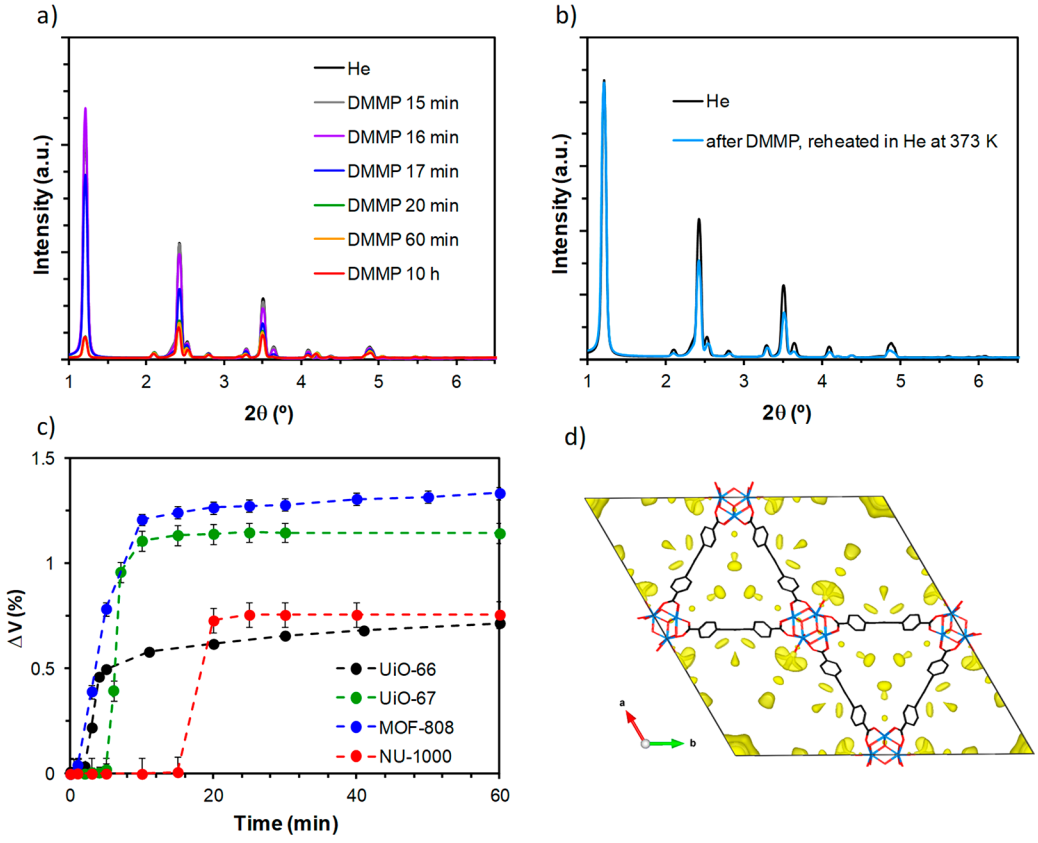

Figure 3. (a) In situ PXRD data of NU-1000 collected during the exposure to DMMP showing the peak intensity changing and peak position shifting toward lowered angles indicative of DMMP adsorbed within the pore space. (b) Comparison of the PXRD pattern of NU-1000 before and after attempted DMMP removal. (c) Evolution of UiO-66, UiO-67, MOF-808, and NU-1000 unit cell volumes with the dosing of DMMP extracted with LeBail fit from time-resolved in situ data. (d) Difference Fourier electron density map of DMMP-treated NU-1000 after 10 h. Zr = blue, C = black, and O = red. Hydrogen atoms have been removed for clarity. Electron density isosurface is drawn at 0.3 $\bar{e}/Å^3$ in yellow color. Reprinted with permission from ref 71. Copyright 2017 American Chemical Society.

tively unsaturated Zr^{4+} centers available, which facilitate nucleophilic hydrolysis of Sarin and DMCP. PXRD data was used here to support the decomposition and loss of long-range order during the reaction.[69] Arcibar-Orozco et al. published a study of decomposition/mineralization of DMCP by copper hydroxyl nitrate and a copper hydroxyl nitrate/graphite oxide composite.[66] Figure 2 shows the PXRD data collected before and after the reaction, where new phases that formed can be identified by the appearance of respective PXRD peaks. The reactive adsorption of the organophosphate moiety leads to transformation of the initial $Cu_2(OH)_3NO_3$ to $CuCl_2$ and $CuCO_3$, as determined by PXRD peak analysis in the

DOI: 10.1021/acsami.9b19494
ACS Appl. Mater. Interfaces 2020, 12, 14721−14738

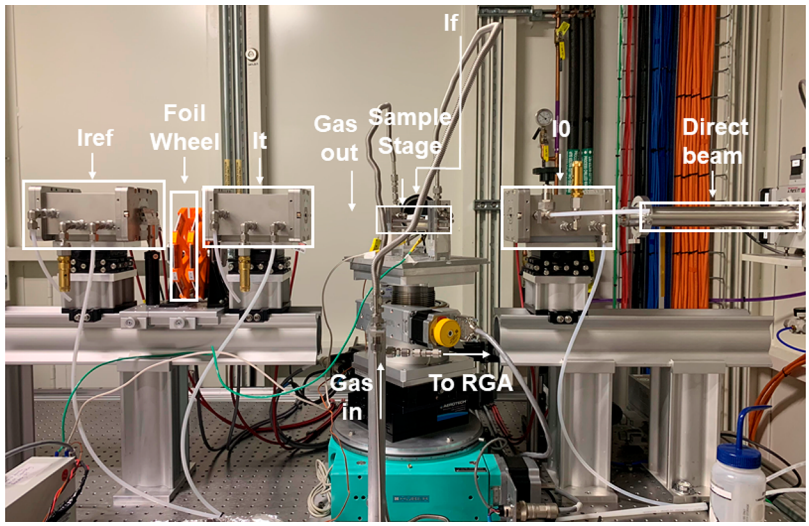

Figure 4. Typical setup of XAFS experiment (shown here is the setup at the QAS beamline of NSLS-II), which contains detectors for incident (I_0), transmitted (I_t), reference (I_{ref}), and fluorescence (I_f) X-ray beams, the sample stage with flow reactor, connected to gas inlet and outlet lines.

recovered sample. The formation of those compounds indicates a replacement of NO_3^- groups by Cl^- or CO_3^{-2}, indicating the mineralization of DMCP and proving that hydroxyl nitrate is an effective protective material against organophosphorus containing CWAs. Further, Stassen et al. used Rietveld refinement to determine the localization of DMMP molecules adsorbed within the pore space of UiO-66-NH_2 to explain the high sensitivity of the material as a sensor for CWAs.[70]

Plonka et al. reported a series of synchrotron-based in situ PXRD experiments on the adsorption and decomposition of DMMP on several Zr-MOFs such as UiO-66, UiO-67, MOF-808, and NU-1000.[71] The use of high-flux synchrotron X-ray facilities allows for rapid acquisition of diffraction data and enables time-resolved studies to follow the structural changes of the material in real time (Figure 3). The nuances in developing and optimizing such a mode of collection allows for the analysis of structural evolution under certain responses. In particular, the extraction of detailed information using such a mode of collection enables us to study the evolution of crystal structural changes during the reaction with simulant molecules. Simple visual examination of the collected data indicates that the adsorbent molecules enter the pore vicinity, and this change is observed in the decrease in the intensity of the low angular reflections (i.e., high *d*-spacing) (Figure 3a). Additional information on the lattice changes under dynamic exposure to DMMP can be clearly seen by the shift in the reflections toward lower 2θ angles indicating unit cell expansion. The comparison of the initial PXRD patterns with patterns after removal of DMMP molecules provides information on the irreversibility of those structural changes induced by DMMP pore adsorption. PXRD data collected from samples treated ex situ also suggested that Zr-MOFs are effective at the removal of CWA simulants from the air.[71] Beyond visual clues, more quantitative information can be extracted from PXRD data with Le Bail analysis, Rietveld refinement and calculation of Fourier density maps. The Le Bail method is a whole structure decomposition approach that extracts unit cell information. Rietveld Refinement is also a non-linear squares minimization of the observed and calculated diffraction profiles with the integrated intensities being experimentally obtained by relevant geometric and structural parameters. Both full profile refinement methods can thus subsequently provide information on the framework volume changes during the adsorption process (Figure 3c). Furthermore, using a difference Fourier analysis, insight into the location of adsorbed and/or products of adsorbent decomposition within the MOFs can be obtained (Figure 3d). Difference density maps are usually calculated using Fourier coefficients, which are the differences between the observed structure factor amplitudes from the experiment and the calculated structure factor amplitudes from the model obtained with Rietveld refinement. A Rietveld refinement approach combining both X-ray and neutron powder diffraction data is also another way to extract more detailed information and solve the crystallographic puzzle.[72]

It is worth mentioning that there are inherent limitations of PXRD, and while it is a powerful tool, it does not provide much information on the samples that lack long-range order, such as nanocrystalline or amorphous materials. Further, catalysis reactions happen on localized sites, and the understanding of local structure is crucial to complement long-range structural information provided by PXRD. Some studies recently emerged that utilize the pair distribution function (PDF) analysis to characterize materials used commonly for CWA decontamination studies. The PDF technique is a total scattering technique that analyzes both Bragg and diffuse scattering enabling the study of short and intermediate range structure of the material even in the presence of significant disorder.[73] Platero-Plats et al. reported the local structural transition of inorganic nodes of NU-1000 and UiO-66 MOFs in the range of temperatures relevant to catalysis applications.[74] Further, King et al. applied PDF analysis in the structure solution of $ZrOH_4$, a very important decontaminant for CWAs, to provide detailed information on local structure and its decomposition at high temperatures.[75]

4. X-RAY ABSORPTION FINE STRUCTURE SPECTROSCOPY

X-ray absorption fine structure (XAFS) spectroscopy is a widely used analytical tool complementary to PDF analysis and employed to investigate electronic structure and local geo-

DOI: 10.1021/acsami.9b19494
ACS Appl. Mater. Interfaces 2020, 12, 14721−14738

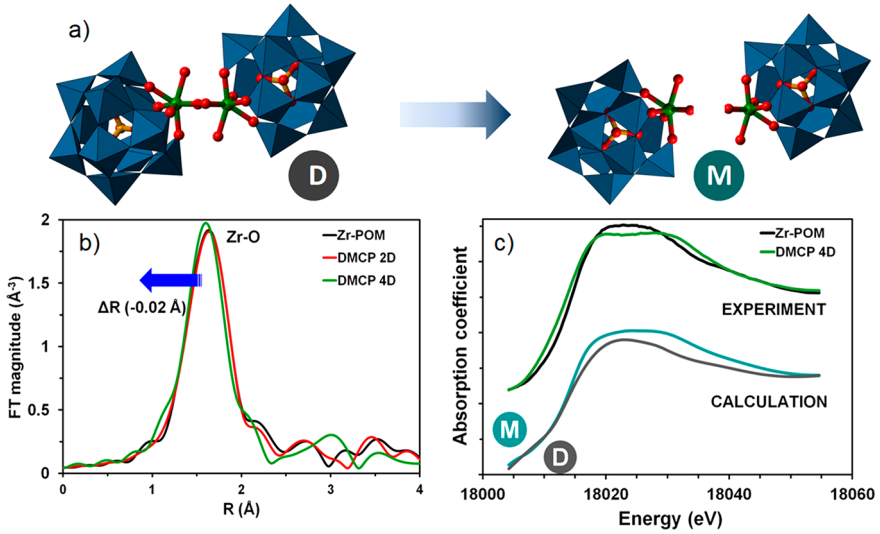

Figure 5. (a) Dissociation of Zr-POM dimers (D) to monomers (M) after the exposure of Zr-POM to DMCP. (b) Fourier transform (FT) magnitudes of the Zr K-edge EXAFS spectra for the pristine and Zr-POM exposed to DMCP for two and 4 days. (c) calculated and experimental Zr K-edge XANES spectra for Zr-POM. The calculated dimer and monomer structure are in agreement with the experimental spectra. Reprinted with permission from ref 69. Copyright 2019 American Chemical Society.

metric properties of specific atomic types in a broad range of materials[76,77] because of the high penetrating power of hard X-rays and the sensitivity to the charge state and local structure of the X-ray absorbing atom.[78] Unlike PDF, XAFS can provide element specific pair distribution. The XAFS spectrum can be divided into two parts that contain complementary information: X-ray absorption near edge structure (XANES) that corresponds to the region from ~30 eV below the absorption edge to 40 eV above and extended X-ray absorption fine structure (EXAFS) that extends ~1000 eV or further past the edge. While XANES is especially sensitive to oxidation state (valence) and geometry environment (e.g., octahedral, tetrahedral coordination) of the absorbing atom,[79] EXAFS provides local structural information, including identities and coordination numbers of nearest neighbors, bond distance and disorder.[78,80] Because of the presence of different types of metal centers in many kinds of filtration materials, XAFS can be useful to detect the changes of chemical states and local bonding structures during their interactions with CWAs and simulants.

While the sensitivity of many characterization techniques for CWA decontamination studies is particularly limited under realistic environmental conditions, XAFS can be applied to such studies with relative ease, because of the high flux of modern synchrotron beamlines, large penetration depth of hard X-rays, and the availability of versatile reactors that can support multiple operating conditions.[81,82] XAFS methods can enable investigation of real-time changes in the agent/simulant uptake, decomposition and filter regeneration processes on a broad range of filtration materials under relevant environmental conditions. A typical in situ/operando XAFS experiment setup is shown in Figure 4.

As a recent example of such correlative studies, Wang et al.,[21] employed in situ XAFS to assess real-time changes of element-specific structure and charge properties of the polyoxoniobate $Cs_8[Nb_6O_{19}]\cdot xH_2O$ (naturally hydrated $Cs_8[Nb_6O_{19}]$ or CsPONb) during reaction with DMMP and observed a change in Nb−O coordination within NbO_6 octahedra. This finding correlated with Raman spectroscopic experiments and DFT modeling results, which indicated that the conversion of DMMP to the (methyl) methylphosphonic acid (M)MPA was accompanied by protonation of Lindqvist unit $[Nb_6O_{19}]^{8-}$ oxygen sites. In situ XAFS also enabled Plonka and co-workers[71] to detect the local structural changes in Zr-based MOFs during reaction with DMMP at the solid−vapor interface. They concluded that the Zr^{4+} environment was affected by DMMP exposure, coupled with the results from the diffraction experiments to indicate that DMMP enters MOF pores, which provided strong evidence that DMMP interacts directly with Zr metal center. The study by Tian and co-workers[69] focused on understanding the mechanism of Sarin and DMCP decomposition on zirconium-substituted POM, $(Et_2NH_2)_8[(\alpha\text{-}PW_{11}O_{39}Zr(\mu\text{-}OH)(H_2O))_2]\cdot 7H_2O$ (Zr-POM). In that work, the exposure of Zr-POM to the warfare agent and the simulant was undertaken by placing the powdered Zr-POM in a sealed jar that was saturated with DMCP (at BNL) and Sarin (at CBC) vapors. That approach enabled direct comparison of the CWA and simulant exposures on filtration materials in real battlefield conditions. XAFS, including XANES modeling by FEFF calculations and EXAFS fitting, provided key insights into local structural changes of Zr-POMs. Specifically, XAFS experiments resulted in the determination of active sites (single Zr sites) during the DMCP decomposition reaction, and provided evidence of transformation of Zr-POM dimers to monomers (Figure 5). By correlating XAFS results with multiple experimental probes and theory, Tian et al., were able to show that the Zr-POM monomer with a coordinatively unsaturated Zr^{4+} center was a key species in a reaction that binds nerve agents and decomposes them via a nucleophilic (general base) hydrolysis mechanism.

5. X-RAY PHOTOELECTRON SPECTROSCOPY

X-ray photoelectron spectroscopy (XPS) and Auger spectroscopy are workhorse surface analytical tools for obtaining chemical and quantitative information from analysis of core−shell spectral photoemission processes. XPS utilizes the photoelectric interactions between a monochromatic photon

DOI: 10.1021/acsami.9b19494
ACS Appl. Mater. Interfaces 2020, 12, 14721−14738

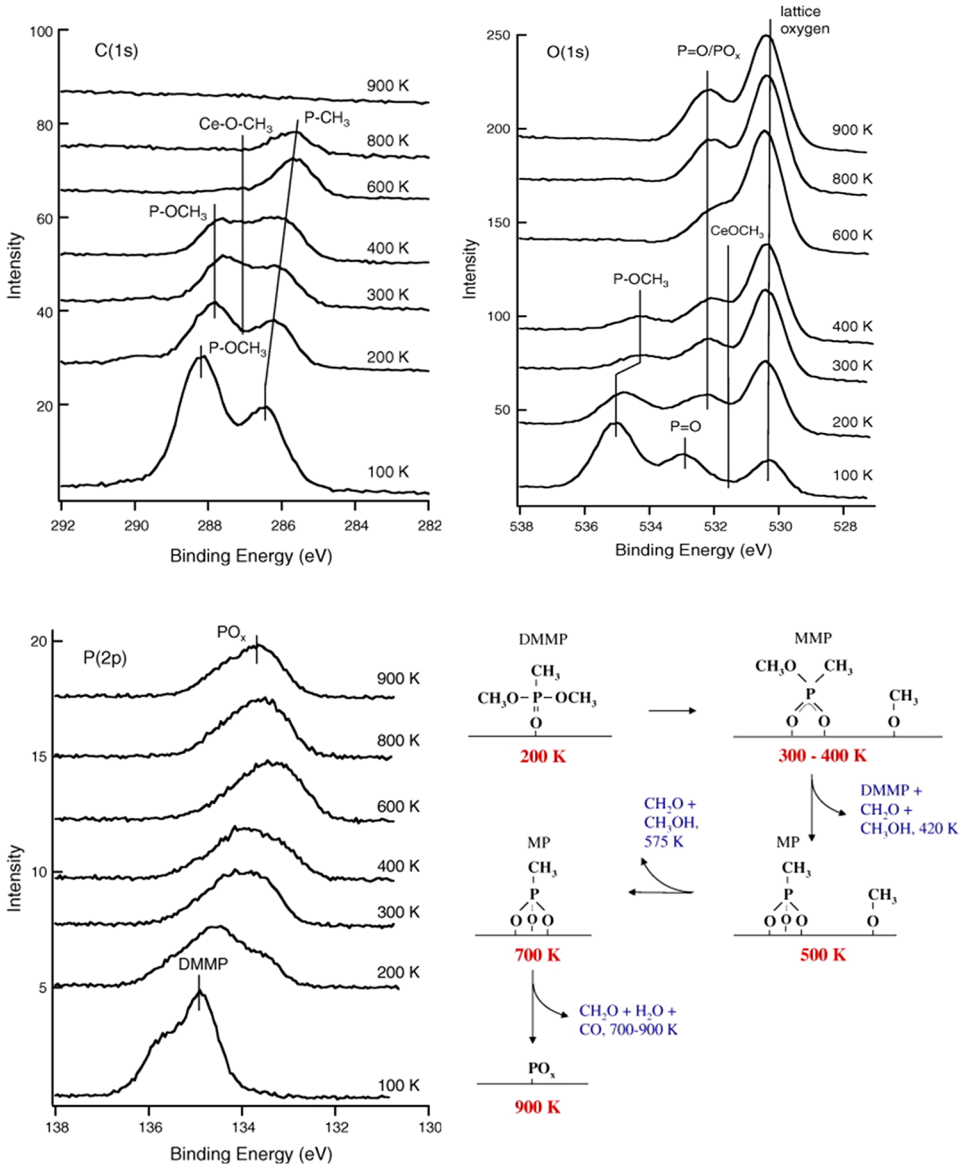

Figure 6. Decomposition of DMMP on CeO_2(111) films as probed in XPS of C (1s), O (1s), and P (2p) regions. Experiments show the initial adsorption of molecular DMMP at 100 K, followed by thermal decomposition to MMP (300−400 K), MP + CH_3O (500 K), and MP (700 K) then PO_x (900 K) species on the CeO_2 surface. Reprinted with permission from ref 91. Copyright 2010 Elsevier.

stream and a material that may be in the form of gas, liquid or solid. The photoemission process is expressed as a relationship between the photoelectron kinetic energy (E_{kin}), electron binding energy (E_b), and correctional factors (work function, ϕ) as follows: $E_{kin} = hc/\lambda - (E_b + \phi)$.[83] This interaction results in the emission of electrons with kinetic energy characteristic to the element, which also provides information on the chemical state and composition of the material studied. Auger electrons are secondary to the core−hole process and occur from the emission of an electron from the same atom and thus detects secondary electrons emitted from a surface.[84] Both spectroscopies provide useful information related to a material's oxidation state and effective charge, splitting of atomic orbitals, and aspects of chemical bonding. The spectroscopic data from these techniques have been widely used in catalysis, polymer chemistry, biological macromolecular (protein, DNA, etc.) adsorption and binding, electrochemistry, metal corrosion and generally provide crucial chemical and physical information on relevant surfaces.[85−89] Because of the chemical sensitivity of the photoemission process to the depth of penetration, XPS can also be used to study particles of different sizes with enhancement of signals from samples with smaller particle sizes and can also distinguish between different elemental species depending on the ionization cross section and pass energy.[84,90]

The chemical sensitivity inherent to XPS is beneficial for nerve agent and other organic phosphonate simulant studies. Chen et al. (Figure 6) followed the structural evolution of DMMP on well-defined ceria and found that the decomposition of DMMP can be tracked carefully on the surface using P(2p), C(1s), and O(1s) regions, including the identification of the oxidation state of cerium between Ce^{3+}/Ce^{4+} in the absence and presence of DMMP. The decomposition of DMMP was performed through thermal annealing resulting in the formation of MMP at 330−400 K, then MP and methanol at 420 K, then MP at 575 K and finally PO_x at 700−900 K.[92] The critical information afforded by XPS

DOI: 10.1021/acsami.9b19494
ACS Appl. Mater. Interfaces 2020, 12, 14721−14738

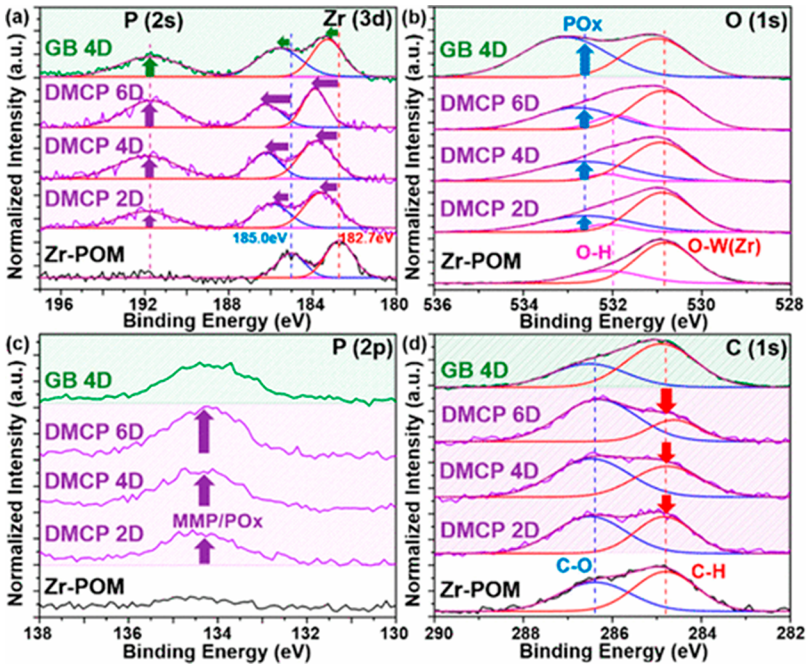

Figure 7. XPS spectra of Zr-POM exposed to GB and DMCP in the (a) P 2s and Zr 3d, (b) O 1s, (c) P 2p, and (d) C 1s regions. Data is collected after exposure to 2 (2D), 4 (4D), and 6 days (6D). Reprinted with permission from ref 69. Copyright 2019 American Chemical Society.

has paved way for many studies that enable researchers to decipher changes because of the adsorption and/or product formation on many classes of materials.[93,94] Head et al. investigated the extent of DMMP adsorption on molybdenum oxide and determined that adsorption of DMMP is favored on defect sites, where oxygen, hydroxyl groups, and under coordinated metal sites are present.[94] Trotochaud and co-workers observed the complete reduction of DMMP into elemental phosphorus on Cu(I)O.[95] Their work suggests that surface bound DMMP undergoes a step by step reduction to atomic phosphorus with the formation of phosphine/phosphinate intermediates. Anion exchange between a coated polymer Au substrate and adsorbed organophosphorus acid simulants of nerve agent was evident by the change in the ratio of the chloride and phosphorus peak intensities.[96,97] Copper, when supported on titania (TiO_2), was shown to furnish the decomposition products (surface hydrogen, methane, and methanol) from DMMP, with methanol generated with highest yield when the Cu coverage increased 10-fold on a titania support.[98] A time-resolved, room-temperature study of DMMP adsorption on copper oxide revealed that molecular DMMP decomposes at room temperature.[99] Pristine titania performed better than titania doped with Au and Pt for the removal and decomposition of DMMP; Ratliff et al. determined that the catalyst is more readily poisoned by the decomposition products in the presence of Pt and Au compared to the pristine titania surface.[100]

XPS was also used to look at the DMCP decomposition process over more complex Zr-POM samples exposed to both Sarin (GB) and DMCP (Figure 7). Here, the time-dependent exposures resulted in a gradual reaction on the surface Zr sites with the DMCP or GB molecule identified by a careful probe of the Zr(3d), P(2p), C (1s), and O(1s) regions.[69]

While there have been several advancements related to surface analysis using XPS, the general fallback lies in the difficulty in calibrating binding energies because of rapid changes in chemical state with thermal annealing. In addition, working with strongly insulating samples is not trivial, and spectrometer calibrations between different instruments are needed to provide a good comparison of related systems of interest. Because of these complexities, several other techniques should be used in tandem with the mindset of a global correlative approach to provide more rigorous quantitative information.

6. NUCLEAR MAGNETIC RESONANCE

Nuclear magnetic resonance (NMR) is a widely utilized analytical technique for many aspects of chemistry because it gives a unique signal for each NMR-active nucleus in a distinct chemical environment. As a result, it is generally straightforward to differentiate and quantify the various compounds present in a reaction including the conversion of chemical warfare agents to nontoxic products. Many studies on the decontamination of both nerve agents and blister agents involve some form of NMR in their analysis.[101,102] Typically, this involves ^{1}H, ^{13}C, ^{19}F, or ^{31}P NMR to follow the conversion of reactants to products in solution. Such analyses help establish the reaction kinetics and product selectivity for both homogeneous and heterogeneous systems. In addition to the traditional one-dimensional spectra listed above, two-dimensional nuclear correlation methods can be used to provide additional structural information.[103−105]

Beyond the frequent use of NMR to follow reaction conversion, NMR techniques can provide insight into key intramolecular/intermolecular interactions.[106−108] For example, Hill and co-workers used ^{31}P NMR to attribute substantial changes in reactivity of Zr-POM for nerve agent simulant hydrolysis to interactions with the solution buffer.[107] In the presence of increasing concentrations of sodium acetate ($NaAc_i$) and phosphate buffer (NaP_i), the chemical shift corresponding to the phosphorus center in the catalyst changes and becomes broadened consistent with a strong interaction between the buffer molecules and the catalyst. In the acetate

DOI: 10.1021/acsami.9b19494
ACS Appl. Mater. Interfaces 2020, 12, 14721−14738

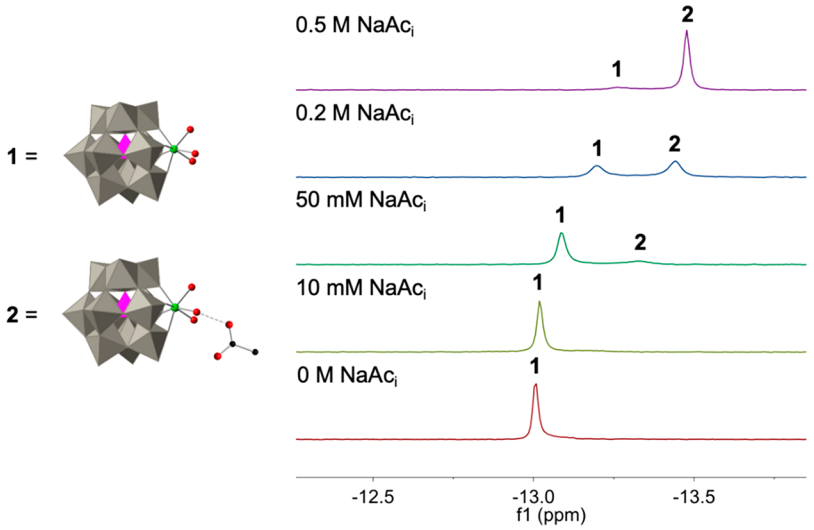

Figure 8. Shifts in the ^{31}P NMR (600 MHz NMR, 1024 scans, 85% H_3PO_4 internal standard) of the polyoxometalate hydrolysis catalyst, [α-$PW_{11}O_{39}Zr(OH)(H_2O)_2]^{4-}$ (**1**), in the presence of different concentrations of sodium acetate buffer ($NaAc_i$). Conditions: 2.5 mM **1**, varied concentration of $NaAc_i$, pH = 4.8, varied concentration of $NaClO_4$ such that the ionic strength was 0.5 M in all cases. Polyhedral representations: WO_6, gray octahedra; PO_4, purple tetrahedra; Zr, green; O, red. Adapted with permission from ref 107. Copyright 2018 American Chemical Society.

form, additional peaks form, which results from acetate binding to the catalyst (Figure 8). Variable temperature ^{31}P NMR helped confirm the bound and unbound forms are in equilibrium with one another. This information on catalyst interactions with other species is critical for better understanding the reaction mechanism and designing improved catalyst systems in the future.

For many decontamination materials, the incorporation of a solvent is impractical, and thus, reactivity must be studied at the gas−solid interface. While NMR is typically done under homogeneous conditions, cross-polarization magic-angle-spinning solid-state NMR (CPMAS SS-NMR) has allowed the in situ study of gas−solid reactions.[109−111] Rigid solid materials (crystalline or amorphous) exhibit very broad NMR signals due to extensive dipolar coupling, chemical shift anisotropy and quadrupolar interactions.[112] However, high-resolution NMR signals can be obtained for liquids (CWAs) adsorbed into/on solid materials using solid state MAS NMR, which helps reduce many of these broadening interactions. "Magic angle" refers to an angle of 54.7° between the rotor spinning axis and the direction of magnetic field.[113] When a sample is spun at this particular angle at fast speeds, motional averaging reduces the inhomogeneities in the sample and narrows the otherwise broad adsorbate signals,[114] which allow for the quantitative determination of CWA decontamination and enhanced ability to identify reaction products on the sorbent materials.

In situ kinetic data can also be measured by taking time-dependent data points. For example, Farha and co-workers were able to use ^{31}P MAS NMR to follow the decomposition of the nerve agent, Soman, over NU-1000 under 50% relative humidity.[115] Further, MAS NMR can also be used to help characterize postsynthetic modifications to heterogeneous catalysts.[20] With both MAS NMR and traditional solution experiments, NMR techniques provide critical information on reaction conversion and important intermolecular and intramolecular interactions. Wagner and co-workers studied room-temperature reactions of CWAs on various commercially available metal oxides, including CaO,[116] MgO,[117] Al_2O_3,[118] TiO_2,[119,120] and $Zr(OH)_4$,[121] using MAS NMR. Reaction of nerve agents GB, GD, and venomous agent X (VX) on these metal oxides was conveniently measured using ^{31}P MAS NMR and typically generated corresponding nontoxic phosphonates chemically bound to the metal surfaces.[14] Decontamination of HD on metal oxides was measured with ^{13}C MAS NMR using ^{13}C-labeled HD which was needed because of the extremely low sensitivity to nonlabeled mustard gas (HD). Reaction of HD typically yielded both hydrolysis and elimination products. More recently, MAS NMR has also been used to study the decontamination of CWA on other MOFs.[53] All three agents (GD, VX, HD) were shown to be detoxified by CuBTC with relatively slow rates, with half-lives over 1 d for GD and VX and 13 h for HD.[122] Decontamination of CWAs by the highly chemically and thermally stable Zr-MOFs has also been studied using MAS NMR. For example, nerve agents were decontaminated by UiO-66-NH_2 and the rate increases with UiO-66-NH_2 defect concentration.[123] As seen with metal oxides, only the nontoxic phosphonic acid products were observed. Besides metal oxides and MOFs, MAS NMR has been used to study the reactivity of CWAs on many other materials, such as concrete, soil, activated charcoal, zeolites, and reactive polymers.[124−129] MAS NMR also allows facile investigation of the effects of water/moisture on decontamination. Sorbent materials can be spiked with various amounts of water or prehumidified at different relative humidity and packed into the rotor, followed by agent dosing. While water often plays an important role in agent decontamination, the precise roles of surface hydroxyls and physisorbed water in the hydrolysis of agent are varied and are not always clear among different agents and materials. Generally, wetted sorbents are more reactive toward CWAs than dry ones. MAS NMR can also effectively distinguish between mobile and immobilized reaction products. When products are weakly bound (physisorbed) to the sorbents, their signals are often narrow and sharp. On the other hand, when CWAs react directly with the matrix and are chemically bound to metal centers, the product signals are often very broad. As a result, dry sorbents typically produce broader product peaks than wetted ones.

DOI: 10.1021/acsami.9b19494
ACS Appl. Mater. Interfaces 2020, 12, 14721−14738

Even though MAS solid-state NMR is a powerful technique for measuring the kinetics of agent decontamination on sorbent materials, the results should be analyzed carefully. For example, the high spinning speed required by MAS NMR can enhance diffusion, causing faster reaction rates than those obtained under nonspinning conditions. However, the spinning effect is not general for all materials and is highly dependent on both the CWA and solid sorbent. For example, reaction of HD on KF/Al_2O_3 sorbent[130] or CuBTC[122] occurs faster at higher MAS spinning speeds. On the other hand, no such effect was observed for VX on KF/Al_2O_3 wetted with water,[131] yet centrifugation effects were observed for VX on KF/Al_2O_3 in the presence of heptane.[132]

MAS NMR has therefore been shown to be a valuable method for studying the adsorption and reaction mechanisms of CWAs on adsorptive and reactive sorbents, however, care must be used to consider the effects of diffusion in to pores and any solubility due to added solvent. Finally, one must consider the drawback of the challenge of working with paramagnetic species that can increase relaxation rates orders of magnitude with proportional peak broadening.

7. RAMAN SPECTROSCOPY

Raman spectroscopy is an inelastic scattering technique that can be used as a probe to study solids, liquids, and gases.[133] Inelastic scattering is a two-photon process that involves the annihilation and the creation of a photon.[134] A Raman signal arises due to changes in the polarizability of a bond during molecular vibration.[135] In a typical Raman experiment, a monochromatic coherent beam of light is transmitted through a sample and undergoes elastic and inelastic scattering. The inelastic scattering is collected and results in a Raman spectrum, which records the scattered radiation as a function of wavenumber, Raman shift, or frequency.[136] A fiber-optic-based Raman spectrometer coupled with a charge-coupled device detector is one of the most commonly used Raman instruments.[137−140] The intensity of the scattering process is correlated with the strength of the coupling of light with molecular vibration. A typical Raman active vibrational mode of a molecule occurs in the 30−3200 cm^{-1} interval. Raman spectroscopy has been particularly used in determining the lattice dynamics and crystallinity of several materials, such as carbon-based,[141,142] metal oxides,[143,144] and polymers.[145,146] Raman spectroscopy can also be used in a time-resolved manner to track the structural changes under in situ conditions.[147] In particular, Raman has been useful in identifying structures, vibrational modes and molecular conformations, as well as bond orientations of organo-phosphorus compounds in their pure form or when adsorbed onto surfaces.[148−152] Depending on the excitation energies, laser power, signal-to-noise ratio, and integration time, many fingerprint regions could be distinguished.[153,154] For example, Choi et al. showed, using principal component analysis applied to Raman spectra, that nerve agents with similar molecular structures can be easily distinguished.[155] Wang et al. identified the adsorption of gaseous dimethyl methylphosphonate and studied the evolution of reaction productions on CsPONb as a function of exposure time (Figure 9).[21] They identified a key intermediate that enables the hydrolysis of dimethyl methyl phosphonate.[21]

While Raman spectroscopy can be useful in gauging the changes with respect to the reactant and the surface, the limitations of Raman as a probing technique arise when the molecule of interest is solvated because Raman spectroscopy is not very sensitive to hydrogen bonding interactions. This factor generally limits the quantitative information obtainable from Raman studies on wet or hydrated materials.

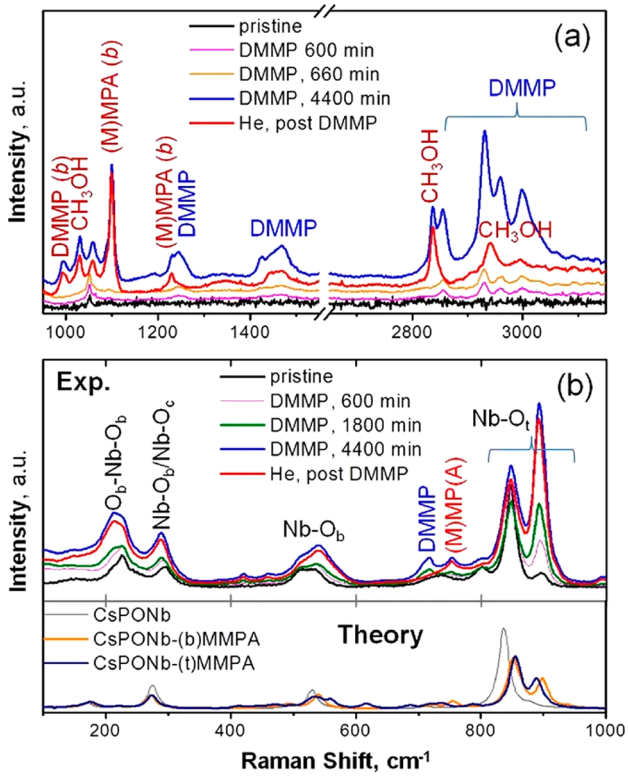

Figure 9. Raman spectra of the reaction system, before reaction (pristine), over the course of stream-feeding of a DMMP/He gas mixture, and in a helium stream following DMMP treatment of a powder sample of $Cs_8[Nb_6O_{19}]$. (a) Spectral region: 950−1550 and 2650−3150 cm^{-1}. (b) Spectral region: 100−1000 cm^{-1}. Bottom panel illustrates theory-predicted Raman signatures for the $Cs_8[Nb_6O_{19}]$ (CsPONb) and CsPONb bound to MMPA (CsPONb-MMPA) at bridging (b) and terminal (t) sites. Reprinted with permission from ref 21. Copyright 2017 Springer Nature Ltd.

8. INFRARED SPECTROSCOPY

Infrared (IR) spectroscopy is a powerful tool that probes chemical functional groups in many materials. IR spectroscopy can be used to probe the chemistry at interfaces and thus help to elucidate interaction mechanisms, polymerization progression, hydrogen bonding interactions in macromolecules, organic compounds, and small probe molecules like CO, NO, and NH_3.[156−158] There are several modes of spectral collection useful for in situ characterization that include: attenuated total reflectance (ATR), diffuse reflectance infrared Fourier transform spectroscopy (DRIFTS), and transmission IR. ATR uses a crystal that enhances the peak intensity of powder or liquid samples using a bench-to-transmission mode while DRIFTS is an internal total reflection application that is used to enhance signal in polycrystalline samples and nonabsorbing or weakly scattering powders. Transmission IR is a technique that measures the absorption of IR radiation by a material (solid, liquid, or gas). A typical spectrum displays the amount of light absorbed or transmitted against wavenumber. Assignments of IR bands are universally documented and referenced for a wide class of organic compounds, with some

DOI: 10.1021/acsami.9b19494
ACS Appl. Mater. Interfaces 2020, 12, 14721−14738

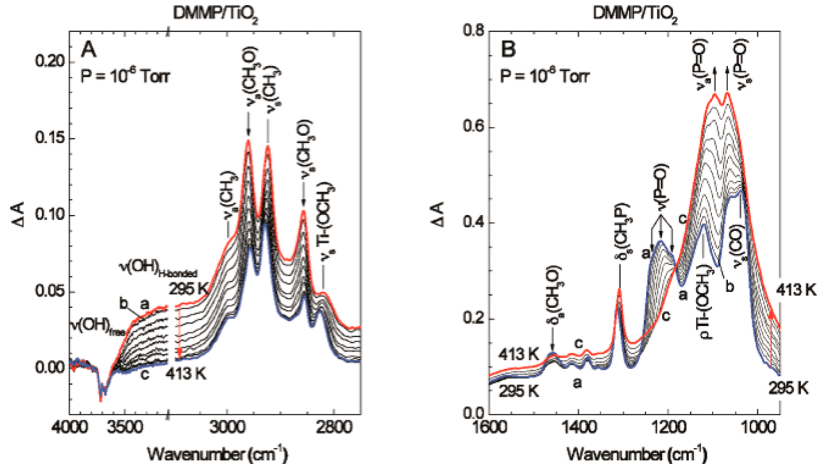

Figure 10. Difference IR spectra of titania nanoparticles precovered with DMMP (0.6 Torr); the spectrum of the clean titania obtained at room temperature before DMMP adsorption was subtracted from each spectrum. Spectra A were obtained after 70 min of prolonged exposure to DMMP and evacuation. Spectra B were obtained during sample heating from 305 to 400 K at a rate of 12 K/min. For each spectrum, 100 scans were averaged; the collection time per spectrum was 30 s. Reproduced with permission from ref 165. Copyright 2009 American Chemical Society.

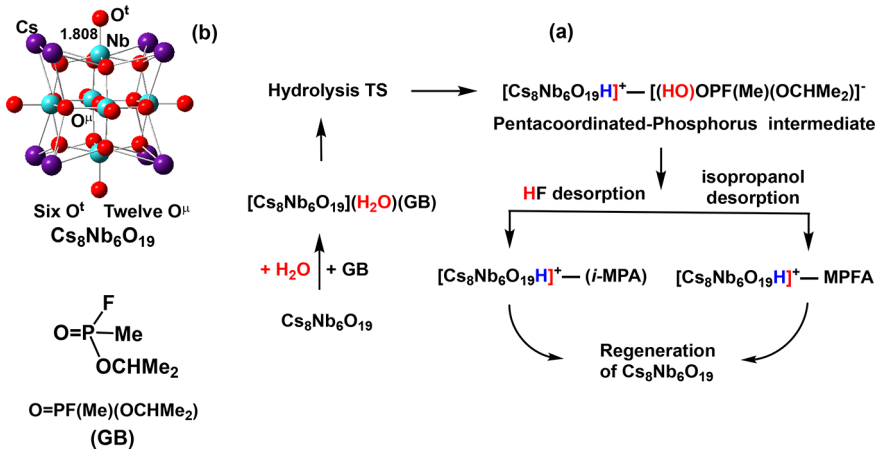

Figure 11. Schematic presentation of (a) the mechanism of Sarin (GB) hydrolysis facilitated by polyoxoniobate, CsPONb, as well as (b) regeneration of CsPONb. Adapted from ref 33 with permission from The Royal Society of Chemistry.

variations in the fine structural details, which may add a level of complexity to the task of spectral analysis in difficult cases.[159]

IR remains an essential tool for the determination of agent-filtration material interactions.[160−163] Gordon and co-workers determined that DMMP decomposition on different particle sizes of Y_2O_3 nanoparticles results in different decomposition behaviors.[161] They have also shown that Y_2O_3 nanoparticles interact with DMMP strongly via the P═O bonds.[161] Moss et al. followed the photoassisted decomposition of DMMP using DRIFTS over TiO_2 and found that this catalyst favors the decomposition via cleavage of the P−OCH_3 with $TiOCH_3$ being the major surface bound decomposition product.[164] Furthermore, they realized that CO_2 is the major product when the system undergoes photodegradation upon exposure to UV light, but the catalyst reactivity was inhibited by surface bound products.[164] A study by Wilmsmeyer et al. on amorphous silica also revealed that the density and chemistry of silanol groups are crucial in binding nerve agent simulants.[163] Similar studies using DMCP discovered that the hydroxyl-rich phase is necessary in decomposing chlorinated species into methanol and hydrochloric acid.[162] Panayotov et al. provided insight into the decomposition pathway of DMMP on titania nanoparticles using infrared spectroscopy (Figure 10).[165] They observed the molecular adsorption of DMMP at room temperature, which upon heating begins to decompose by the loss of the hydroxyl group to afford MPA as an intermediate product at 300−400 K. These processes are assisted by the titania lattice oxygen leading to MP as a final product.[165]

9. COMBINING EXPERIMENTS AND THEORY

The complexity of catalytic decontamination of CWAs requires a multidisciplinary approach for deeper understanding of intimate mechanistic details and solid−multigas interfacial dynamics of the reaction between catalyst and simulant. Modern computation methodologies, such as GGA-DFT, planewave-DFT, various ab initio approaches, MD-simulations methods, as well as hybrid approaches (such as QM/MM, ONIOM, and QM/MM/MD) have proven to be some of the highly effective complementary approaches. Computation allows one to pinpoint controlling factors, such as electro-negativity, electron affinity, pK_a, and size (sterics) of the leaving group, in simulant decontamination by various materials and identifies expandable bond order and bond strength among other chemical descriptors for prediction of

DOI: 10.1021/acsami.9b19494
ACS Appl. Mater. Interfaces 2020, 12, 14721−14738

new and more effective filtration technologies and decontamination materials.

The mechanism for CsPONb-mediated GB decomposition in the presence and absence of ambient gases has been fully identified,[19,32,166] and in both cases the GB hydrolysis by CsPONb has been shown to proceed via a *general-base* hydrolysis mechanism that involves the coadsorption of water and nerve agent molecules and the expulsion of HF or isopropanol (Figure 11). In the presence of ambient gases, the basic terminal (O^t) or bridging (O^μ) oxygen of the polyoxometalate binds the ambient gases and consequently becomes unavailable for the hydrolysis process. Instead, one of O centers of the coordinated ambient gas molecules becomes an active site for hydrolysis. This raises the energy of the stationary points relative to the reactants asymptote and increases the hydrolysis barrier. Regeneration of the catalyst is a highly endergonic process and is the rate-limiting step for GB hydrolytic decontamination, both in the absence and presence of ambient gas molecules. The presence of ambient gas molecules reduces the energy required for the rate-limiting catalyst regeneration (i.e., product elimination) and facilitates catalytic decomposition of CWAs.

Electronic structure calculations have also been extraordinarily successful in revealing atomistic details of the chemistry of MOFs.[167] In particular, DFT calculations of CWAs and surrogate-molecule adsorption and reactions on Zr-MOFs have enabled a very detailed understanding of the success of these materials in decomposing the toxic molecules.[166,168−171] Much as with the hydrolysis of nerve agents in POMs, the calculations indicate the degradation of these molecules in Zr-MOFs involves nucleophilic addition of OH to generate a pentacoordinated phosphorus intermediate that quickly decomposes into products. Experimental evidence combining IR spectroscopy and difference Fourier electron density maps (Figure 3d) show that the phosphorus-containing product of the hydrolysis remains on the MOF after reaction. Moreover, in ultrahigh-vacuum, the product is so strongly bound to the MOF that it cannot be thermally desorbed at temperatures below which the Zr-MOF is stable, that is, the Zr-MOF thermally decomposes before the phosphonate product is removed. Calculations suggest the phosphonate product can interact in a bidentate manner to adjacent Zr sites on the MOF (Figure 12). The good agreement between the calculated and measured IR spectrum of this strongly bound product cautions the Zr-MOF might quickly become inhibited during reaction under low-humidity conditions. Humidity effects and carbon dioxide effects on the degradation of CWA simulants in the presence of MOF-808 were recently demonstrated.[172] Active-site poisoning will therefore need to be fully addressed in next-generation materials.

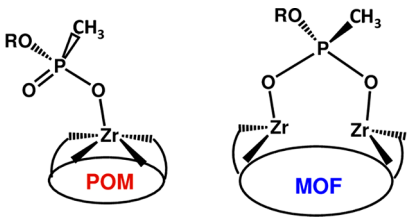

Figure 12. Organophosphorus coordination motif in the Zr-POM (left) and Zr-MOF (right) gas−solid systems under dry conditions.

Also, theory has proven to be invaluable for identifying true nature of active species, as well as pinpoint roles of noncovalent (or weak) interactions facilitating active catalyst formation and simulant decomposition. On the basis of the DFT calculations,[69] we have shown that the active catalyst of Zr-POM (**D**) in the decomposition of GB and DMCP is the monomeric form of Zr-POM. Furthermore, the monomerization of **D** is significantly facilitated by the simulant-catalyst interaction. Indeed, the monomerization of **D**, in the absence of warfare gases requires 38.5 kJ/mol enthalpy. However, the coordination of DMCP and GB molecules to **D** reduces the energy required for monomeric Zr-POM formation to 12.6 and 14.2 kJ/mol, respectively.

These calculations revealed that the decomposition of DMCP by the Zr-POM monomers also occurs via a *general-base* hydrolysis mechanism. A noteworthy aspect of the Zr-POM mediated CWA decomposition is that in the most stable Zr-phosphorus intermediate of the reaction the organophosphorus species is bound to Zr-catalyst by only one Zr−O covalent bond. This bonding motif is very different from the energetically most stable intermediate in Zr-MOFs mediated CWA decontamination under dry conditions, where the OP hydrolysis product is strongly bound to adjacent Zr sites of the MOF in a bidentate fashion (Figure 12).[71,166] The difference in these bonding motifs clearly demonstrates that the energy required to remove phosphate/phosphonate product (which is the rate-limiting step of the entire CWA decomposition in both cases) from the catalyst can be significantly smaller for Zr-POMs than for Zr-MOFs. This finding makes Zr-POMs a promising class of single-site molecular catalyst.

Possibilities for continued synergy between theory and experiment at the vapor/gas interface abound and will no doubt figure significantly in future CWA decomposition studies. For instance, while the MOFs and POMs in this work have precisely controlled composition and structure that restrict the initial adsorption of gases and their reactions on well-established sites (undercoordinated metals, hydroxyl groups, etc.), the materials of the future (polymeric POMs, POM-MOF assemblies, microporous polymers, etc.) might have more heterogeneous and amorphous surfaces, where the initial binding site and subsequent chemistry will be less clear. High-resolution XAFS, IR, and Raman will, therefore, be critical in directing the calculations toward the more important possible binding sites.

DFT calculations rely on approximations that necessarily incur some error. Specifically, the barriers of multistep reaction mechanisms predicted by the calculations would benefit from experimental calibration, which would require time-resolved experiments on a much finer time scale than is currently possible on the systems reviewed in this work. Until such experiments are possible, electronic structure calculations will continue to provide understanding of short-lived intermediates (e.g., the pentacoordinated phosphorus intermediate in nerve-agent hydrolysis) that cannot currently be resolved in the laboratory. Finally, an additional challenge is the simulation of decontamination under more realistic conditions (to correlate structure property relationships and predict material−agent interactions), by incorporating ambient gas molecules (such as CO_2, NO, NO_2, SO_2, and various hydrocarbons), temperature, and gas concentrations.

DOI: 10.1021/acsami.9b19494
ACS Appl. Mater. Interfaces 2020, 12, 14721−14738

10. CONCLUSION

In this Review, we highlighted the challenges toward mechanistic understanding of CWA capture and/or decomposition in realistic battlefield conditions and addressed recent characterization methodologies designed to solve them. The synchrotron techniques, such as X-ray absorption spectroscopy and X-ray diffraction, are particularly powerful in probing the structural and compositional changes of CWA decontamination materials in real working conditions. We have also demonstrated the need for a multimodal, in situ/operando approach enabling comprehensive studies of all components in agent-filter systems. These studies rely on the use of dedicated gas/vapor delivery systems, analysis of reaction products, and ever more frequently, synergy of experiment and theory. A one-fits-all solution to these types of studies does not exist (for example, as demonstrated in this Review, the studies of filtration properties of MOFs and POMs rely on different combinations of techniques) but the community is beginning to appreciate the power of collaborative teams and dedicated research infrastructure for CWA defense studies. One possible direction that can advance research on novel filtration materials could be a consortium of multiple chemical defense research teams from academia, national, and defense laboratories, tasked to provide scientific solutions to investigator needs and train early career researchers in the experimental and theoretical methods. Establishing such consortium (Defense Synchrotron Consortium or DSC) at Brookhaven National Laboratory is in the planning stage at the time of writing of this Review.

AUTHOR INFORMATION

Corresponding Author

*Email: anatoly.frenkel@stonybrook.edu.

ORCID

Anna M. Plonka: 0000-0003-2606-0477
Yiyao Tian: 0000-0002-8148-9375
Sanjaya D. Senanayake: 0000-0003-3991-4232
Djamaladdin G. Musaev: 0000-0003-1160-6131
John R. Morris: 0000-0001-9140-5211
Diego Troya: 0000-0003-4971-4998
Anatoly I. Frenkel: 0000-0002-5451-1207

Author Contributions

A.M.E. and A.I.F. developed the concept and wrote the manuscript. A.M.P., Y.T., S.D.S., W.O.G., A.B., H.W., D.L.C.-W., D.G.M., and D.T. contributed content to different sections of the manuscript. S.D.S., W.O.G., A.B., C.L.H, D.G.M., J.R.M., D.T., and A.I.F. contributed to the discussion and summary presented in the last two sections.

Notes

The authors declare no competing financial interest.

ACKNOWLEDGMENTS

This work is supported by the U.S. Army Research Laboratory and the U.S. Army Research Office under grant number W911NF-15-2-0107. We thank the Defense Threat Reduction Agency for support under program CB3587. Reaction tests at Brookhaven National Laboratory's Chemistry Division were made possible due to the Laboratory Directed Research and Development Program through LDRD 18-047 fund to A.I.F. This research used beamlines 7-BM (QAS), 8-ID (ISS), 8-BM (TES), and 28-ID-2 (XPD) of the National Synchrotron Light Source II, a U.S. DOE Office of Science User Facility operated for the DOE Office of Science by Brookhaven National Laboratory under Contract No. DE-SC0012704. It used 17-BM and 9-BM beamlines of the Advanced Photon Source at Argonne National Laboratory and BL2-2 beamline of the Stanford Synchrotron Radiation Lightsource of the SLAC National Laboratory. Uses of the Argonne Advanced Photon Source and Stanford Synchrotron Radiation Lightsource were supported by DOE under Contracts No. DE-AC02-06CH11357 and DE-AC02-76SF00515, respectively. We acknowledge Cherry L. Emerson Center for Scientific Computation at Emory University and Advance Research Computing at Virginia Tech for providing computational resources and technical support.

REFERENCES

(1) Fitzgerald, G. J. Chemical Warfare and Medical Response During World War I. *Am. J. Public Health* **2008**, *98*, 611−625.

(2) Jung, U.; Elsen, A.; Li, Y.; Smith, J. G.; Small, M. W.; Stach, E. A.; Frenkel, A. I.; Nuzzo, R. G. Comparative in Operando Studies in Heterogeneous Catalysis: Atomic and Electronic Structural Features in the Hydrogenation of Ethylene over Supported Pd and Pt Catalysts. *ACS Catal.* **2015**, *5*, 1539−1551.

(3) Frenkel, A. I.; Rodriguez, J. A.; Chen, J. G. Synchrotron Techniques for In Situ Catalytic Studies: Capabilities, Challenges, and Opportunities. *ACS Catal.* **2012**, *2*, 2269−2280.

(4) Bordiga, S.; Groppo, E.; Agostini, G.; van Bokhoven, J. A.; Lamberti, C. Reactivity of Surface Species in Heterogeneous Catalysts Probed by In Situ X-ray Absorption Techniques. *Chem. Rev.* **2013**, *113*, 1736−1850.

(5) Li, X.; Yang, X.; Zhang, J.; Huang, Y.; Liu, B. In Situ/Operando Techniques for Characterization of Single-Atom Catalysts. *ACS Catal.* **2019**, *9*, 2521−2531.

(6) Mendonca, M. L.; Snurr, R. Q. Screening for Improved Nerve Agent Simulants and Insights into Organophosphate Hydrolysis Reactions from DFT and QSAR Modeling. *Chem. - Eur. J.* **2019**, *25*, 9217−9229.

(7) Gotor, R.; Costero, A. M.; Gil, S.; Parra, M.; Martínez-Máñez, R.; Sancenón, F. A Molecular Probe for the Highly Selective Chromogenic Detection of DFP, a Mimic of Sarin and Soman Nerve Agents. *Chem. - Eur. J.* **2011**, *17*, 11994−11997.

(8) Singh, B.; Prasad, G.; Pandey, K.; Danikhel, R.; Vijayaraghavan, R. Decontamination of Chemical Warfare Agents. *Def. Sci. J.* **2010**, *60*, 428−441.

(9) Khan, A.; Kotta, S.; Ansari, S.; Ali, J.; Sharma, R. Recent Advances in Decontamination of Chemical Warfare Agents. *Def. Sci. J.* **2013**, *63*, 487−496.

(10) Yang, Y. C.; Baker, J. A.; Ward, J. R. Decontamination of Chemical Warfare Agents. *Chem. Rev.* **1992**, *92*, 1729−1743.

(11) Wilson, C.; Cooper, N. J.; Briggs, M. E.; Cooper, A. I.; Adams, D. J. Investigating the Breakdown of the Nerve Agent Simulant Methyl Paraoxon and Chemical Warfare Agents GB and VX Using Nitrogen Containing Bases. *Org. Biomol. Chem.* **2018**, *16*, 9285−9291.

(12) Henych, J.; Janoš, P.; Kormunda, M.; Tolasz, J.; Štengl, V. Reactive Adsorption of Toxic Organophosphates Parathion Methyl and DMMP on Nanostructured Ti/Ce Oxides and their Composites. *Arabian J. Chem.* **2016**, DOI: 10.1016/j.arabjc.2016.06.002.

(13) Hung, W.-C.; Wang, J.-C.; Wu, K.-H. Adsorption and Decomposition of Dimethyl Methylphosphonate (DMMP) on Expanded Graphite/Metal Oxides. *Appl. Surf. Sci.* **2018**, *444*, 330−335.

(14) Wagner, G. W., Decontamination of Chemical Warfare Agents with Nanosize Metal Oxides. *Nanoscale Materials in Chemistry: Environmental Applications*; American Chemical Society, 2010; Vol. *1045*, pp 125−136.

DOI: 10.1021/acsami.9b19494
ACS Appl. Mater. Interfaces 2020, 12, 14721−14738

(15) Panayotov, D. A.; Morris, J. R. Uptake of a Chemical Warfare Agent Simulant (DMMP) on TiO_2: Reactive Adsorption and Active Site Poisoning. *Langmuir* **2009**, *25*, 3652−3658.
(16) Florent, M.; Giannakoudakis, D. A.; Wallace, R.; Bandosz, T. J. Mixed CuFe and ZnFe (hydr)oxides as Reactive Adsorbents of Chemical Warfare Agent Surrogates. *J. Hazard. Mater.* **2017**, *329*, 141−149.
(17) Janoš, P.; Henych, J.; Pelant, O.; Pilařová, V.; Vrtoch, L.; Kormunda, M.; Mazanec, K.; Štengl, V. Cerium Oxide for the Destruction of Chemical Warfare Agents: A Comparison of Synthetic Routes. *J. Hazard. Mater.* **2016**, *304*, 259−268.
(18) Štengl, V.; Grygar, T. M.; Bludská, J.; Opluštil, F.; Němec, T. Mesoporous Iron−Manganese Oxides for Sulphur Mustard and Soman Degradation. *Mater. Res. Bull.* **2012**, *47*, 4291−4299.
(19) Kaledin, A. L.; Troya, D.; Karwacki, C. J.; Balboa, A.; Gordon, W. O.; Morris, J. R.; Mitchell, M. B.; Frenkel, A. I.; Hill, C. L.; Musaev, D. G. Key Mechanistic Details of Paraoxon Decomposition by Polyoxometalates: Critical Role of Para-nitro Substitution. *Chem. Phys.* **2019**, *518*, 30−37.
(20) Sullivan, K. P.; Neiwert, W. A.; Zeng, H.; Mehta, A. K.; Yin, Q.; Hillesheim, D. A.; Vivek, S.; Yin, P.; Collins-Wildman, D. L.; Weeks, E. R.; Liu, T.; Hill, C. L. Polyoxometalate-based Gelating Networks for Entrapment and Catalytic Decontamination. *Chem. Commun.* **2017**, *53*, 11480−11483.
(21) Wang, Q.; Chapleski, R. C.; Plonka, A. M.; Gordon, W. O.; Guo, W.; Nguyen-Phan, T.-D.; Sharp, C. H.; Marinkovic, N. S.; Senanayake, S. D.; Morris, J. R.; Hill, C. L.; Troya, D.; Frenkel, A. I. Atomic-Level Structural Dynamics of Polyoxoniobates during DMMP Decomposition. *Sci. Rep.* **2017**, *7*, 773.
(22) Dong, J.; Hu, J.; Chi, Y.; Lin, Z.; Zou, B.; Yang, S.; Hill, C. L.; Hu, C. A Polyoxoniobate−Polyoxovanadate Double-Anion Catalyst for Simultaneous Oxidative and Hydrolytic Decontamination of Chemical Warfare Agent Simulants. *Angew. Chem., Int. Ed.* **2017**, *56*, 4473−4477.
(23) Kim, E.; Huang, K.; Tomala, A.; Matthews, S.; Strubell, E.; Saunders, A.; McCallum, A.; Olivetti, E. Machine-Learned and Codified Synthesis Parameters of Oxide Materials. *Sci. Data* **2017**, *4*, 170127.
(24) Bailey, M. M.; Heddleston, J. M.; Davis, J.; Staymates, J. L.; Hight Walker, A. R. Functionalized, Carbon Nanotube Material for the Catalytic Degradation of Organophosphate Nerve agents. *Nano Res.* **2014**, *7*, 390−398.
(25) Osovsky, R.; Kaplan, D.; Nir, I.; Rotter, H.; Elisha, S.; Columbus, I. Decontamination of Adsorbed Chemical Warfare Agents on Activated Carbon Using Hydrogen Peroxide Solutions. *Environ. Sci. Technol.* **2014**, *48*, 10912−10918.
(26) Dinu, C. Z.; Borkar, I. V.; Bale, S. S.; Zhu, G.; Sanford, K.; Whited, G.; Kane, R. S.; Dordick, J. S. Enzyme-Nanotube-Based Composites Used for Chemical and Biological Decontamination. *ACS Symp. Ser.* **2010**, *1043*, 103−107.
(27) Giannakoudakis, D. A.; Seredych, M.; Rodríguez-Castellón, E.; Bandosz, T. J. Mesoporous Graphitic Carbon Nitride-Based Nanospheres as Visible-Light Active Chemical Warfare Agents Decontaminant. *Chem. Nano Mat* **2016**, *2*, 268−272.
(28) Giannakoudakis, D. A.; Hu, Y.; Florent, M.; Bandosz, T. J. Smart textiles of MOF/g-C3N4 Nanospheres for the Rapid Detection/Detoxification of Chemical Warfare Agents. *Nanoscale Horizons* **2017**, *2*, 356−364.
(29) Gil-San-Millan, R.; López-Maya, E.; Hall, M.; Padial, N. M.; Peterson, G. W.; DeCoste, J. B.; Rodríguez-Albelo, L. M.; Oltra, J. E.; Barea, E.; Navarro, J. A. R. Chemical Warfare Agents Detoxification Properties of Zirconium Metal−Organic Frameworks by Synergistic Incorporation of Nucleophilic and Basic Sites. *ACS Appl. Mater. Interfaces* **2017**, *9*, 23967.
(30) Cai, S.; Li, W.; Xu, P.; Xia, X.; Yu, H.; Zhang, S.; Li, X. In situ construction of metal−organic framework (MOF) UiO-66 film on Parylene-Patterned Resonant Microcantilever for Trace Organophosphorus Molecules Detection. *Analyst* **2019**, *144*, 3729−3735.
(31) Gil-San-Millan, R.; López-Maya, E.; Platero-Prats, A. E.; Torres-Pérez, V.; Delgado, P.; Augustyniak, A. W.; Kim, M. K.; Lee, H. W.; Ryu, S. G.; Navarro, J. A. R. Magnesium Exchanged Zirconium Metal−Organic Frameworks with Improved Detoxification Properties of Nerve Agents. *J. Am. Chem. Soc.* **2019**, *141* (30), 11801−11805.
(32) Clarkson, E. D.; Gordon, R. K. Chapter 76—Rapid Decontamination of Chemical Warfare Agents from the Skin. *Handbook of Toxicology of Chemical Warfare Agents*, 2nd ed.; Gupta, R. C., Ed.; Academic Press: Boston, 2015; pp 1127−1139.
(33) Kaledin, A. L.; Driscoll, D. M.; Troya, D.; Collins-Wildman, D. L.; Hill, C. L.; Morris, J. R.; Musaev, D. G. Impact of Ambient Gases on the Mechanism of [Cs(8)Nb(6)O(19)]-Promoted Nerve-Agent Decomposition. *Chem. Sci.* **2018**, *9*, 2147−2158.
(34) Das, R.; Ali, E.; Abd Hamid, S. B. Current Applications of X-ray Powder Diffraction—A review. *Reviews on Advanced Materials Science* **2014**, *38*, 95−109.
(35) Houšková, V.; Štengl, V.; Bakardjieva, S.; Murafa, N.; Kalendova, A.; Opluštil, F. Zinc oxide Prepared by Homogeneous Hydrolysis with Thioacetamide, its Destruction of Warfare Agents, and Photocatalytic Activity. *J. Phys. Chem. A* **2007**, *111*, 4215−4221.
(36) Islamoglu, T.; Ortuño, M. A.; Proussaloglou, E.; Howarth, A. J.; Vermeulen, N. A.; Atilgan, A.; Asiri, A. M.; Cramer, C. J.; Farha, O. K. Presence versus Proximity: the Role of Pendant Amines in the Catalytic Hydrolysis of a Nerve Agent Simulant. *Angew. Chem., Int. Ed.* **2018**, *57*, 1949−1953.
(37) Holdren, S.; Tsyshevsky, R.; Fears, K.; Owrutsky, J.; Wu, T.; Wang, X.; Eichhorn, B. W.; Kuklja, M. M.; Zachariah, M. R. Adsorption and Destruction of the G-Series Nerve Agent Simulant Dimethyl Methylphosphonate on Zinc Oxide. *ACS Catal.* **2019**, *9*, 902−911.
(38) Walling, S. A.; Notman, S.; Watts, P.; Govan, N.; Provis, J. L. Portland Cement Based Immobilisation/Destruction of Chemical Weapon Agent Degradation Products. *Ind. Eng. Chem. Res.* **2019**, *58*, 10383−10393.
(39) Sundarrajan, S.; Ramakrishna, S. Fabrication of Nanocomposite Membranes from Nanofibers and Nanoparticles for Protection Against Chemical Warfare Simulants. *J. Mater. Sci.* **2007**, *42*, 8400−8407.
(40) Prasad, G. K.; Mahato, T. H.; Singh, B.; Ganesan, K.; Pandey, P.; Sekhar, K. Detoxification Reactions of Sulphur Mustard on the Surface of Zinc Oxide Nanosized rods. *J. Hazard. Mater.* **2007**, *149*, 460−464.
(41) Jeon, S.; Balow, R. B.; Daniels, G. C.; Ko, J. S.; Pehrsson, P. E. Conformal Nanoscale Zirconium Hydroxide Films for Decomposing Chemical Warfare Agents. *ACS Appl. Nano Mater.* **2019**, *2*, 2295−2307.
(42) Howarth, A. J.; Liu, Y.; Li, P.; Li, Z.; Wang, T. C.; Hupp, J. T.; Farha, O. K. Chemical, Thermal and Mechanical Stabilities of Metal−Organic Frameworks. *Nat. Rev. Mater.* **2016**, *1*, 15018.
(43) Yekta, S.; Sadeghi, M.; Mirzaei, D.; Zabardasti, A.; Farhadi, S. Removal of Nerve Agent Sarin Simulant from Aqueous Solution using the ZSM-5/CoFe 2 O 4 NPs Adsorbent. *J. Iran. Chem. Soc.* **2019**, *16*, 269−282.
(44) Grandcolas, M.; Louvet, A.; Keller, N.; Keller, V. Layer-by-layer Deposited Titanate-Based Nanotubes for Solar Photocatalytic Removal of Chemical Warfare Agents from Textiles. *Angew. Chem., Int. Ed.* **2009**, *48*, 161−164.
(45) Carniato, F.; Bisio, C.; Psaro, R.; Marchese, L.; Guidotti, M. Niobium (V) Saponite Clay for The Catalytic Oxidative Abatement of Chemical Warfare Agents. *Angew. Chem., Int. Ed.* **2014**, *53*, 10095−10098.
(46) Lian, X.; Yan, B. Trace Detection of Organophosphorus Chemical Warfare Agents in Wastewater and Plants by Luminescent UIO-67 (Hf) and Evaluating the Bioaccumulation of Organophosphorus Chemical Warfare Agents. *ACS Appl. Mater. Interfaces* **2018**, *10*, 14869−14876.
(47) Štengl, V.; Grygar, T. M.; Opluštil, F.; Němec, T. Ge4+ doped TiO2 for stoichiometric degradation of warfare agents. *J. Hazard. Mater.* **2012**, *227*, 62−67.

DOI: 10.1021/acsami.9b19494
ACS Appl. Mater. Interfaces 2020, 12, 14721−14738

(48) Li, P.; Moon, S.-Y.; Guelta, M. A.; Harvey, S. P.; Hupp, J. T.; Farha, O. K. Encapsulation of a Nerve agent Detoxifying Enzyme by a Mesoporous Zirconium Metal−Organic Framework Engenders Thermal and Long-Term Stability. *J. Am. Chem. Soc.* **2016**, *138*, 8052−8055.
(49) Singh, V. V.; Jurado-Sánchez, B.; Sattayasamitsathit, S.; Orozco, J.; Li, J.; Galarnyk, M.; Fedorak, Y.; Wang, J. Multifunctional silver-exchanged zeolite micromotors for catalytic detoxification of chemical and biological threats. *Adv. Funct. Mater.* **2015**, *25* (14), 2147−2155.
(50) Mahato, T.; Prasad, G.; Singh, B.; Acharya, J.; Srivastava, A.; Vijayaraghavan, R. Nanocrystalline Zinc Oxide for the Decontamination of Sarin. *J. Hazard. Mater.* **2009**, *165*, 928−932.
(51) Patterson, A. The Scherrer Formula for X-ray Particle Size Setermination. *Phys. Rev.* **1939**, *56*, 978.
(52) Miranda, M. A. R.; Sasaki, J. M. The Limit of Application of the Scherrer Equation. *Acta Crystallogr., Sect. A: Found. Adv.* **2018**, *74*, 54−65.
(53) Mondloch, J. E.; Katz, M. J.; Isley, W. C., III; Ghosh, P.; Liao, P.; Bury, W.; Wagner, G. W.; Hall, M. G.; DeCoste, J. B.; Peterson, G. W.; et al. Destruction of Chemical Warfare Agents Using Metal−Organic Orameworks. *Nat. Mater.* **2015**, *14*, 512.
(54) Liu, Y.; Buru, C. T.; Howarth, A. J.; Mahle, J. J.; Buchanan, J. H.; DeCoste, J. B.; Hupp, J. T.; Farha, O. K. Efficient and Selective Oxidation of Sulfur Mustard using Singlet Oxygen Generated by a Pyrene-Based Metal−Organic Framework. *J. Mater. Chem. A* **2016**, *4*, 13809−13813.
(55) Moon, S. Y.; Liu, Y.; Hupp, J. T.; Farha, O. K. Instantaneous Hydrolysis of Nerve-Agent Simulants with a Six-Connected Zirconium-Based Metal−Organic Framework. *Angew. Chem., Int. Ed.* **2015**, *54*, 6795−6799.
(56) Peterson, G. W.; Browe, M. A.; Durke, E. M.; Epps, T. H., III Flexible SIS/HKUST-1 Mixed Matrix Composites as Protective Barriers Against Chemical Warfare Agent Simulants. *ACS Appl. Mater. Interfaces* **2018**, *10*, 43080−43087.
(57) Howarth, A. J.; Buru, C. T.; Liu, Y.; Ploskonka, A. M.; Hartlieb, K. J.; McEntee, M.; Mahle, J. J.; Buchanan, J. H.; Durke, E. M.; Al-Juaid, S. S.; et al. Postsynthetic Incorporation of a Singlet Oxygen Photosensitizer in a Metal−Organic Framework for Fast and Selective Oxidative Detoxification of Sulfur Mustard. *Chem. - Eur. J.* **2017**, *23*, 214−218.
(58) Liu, Y.; Howarth, A. J.; Hupp, J. T.; Farha, O. K. Selective Photooxidation of a Mustard-Gas Simulant Catalyzed by a Porphyrinic Metal−Organic Framework. *Angew. Chem., Int. Ed.* **2015**, *54*, 9001−9005.
(59) Atilgan, A.; Islamoglu, T.; Howarth, A. J.; Hupp, J. T.; Farha, O. K. Detoxification of a Sulfur Mustard Simulant Using a BODIPY-Functionalized Zirconium-Based Metal−Organic Framework. *ACS Appl. Mater. Interfaces* **2017**, *9*, 24555−24560.
(60) Pereira, C. F.; Liu, Y.; Howarth, A.; Figueira, F.; Rocha, J.; Hupp, J. T.; Farha, O. K.; Tomé, J. P.; Almeida Paz, F. A. Detoxification of a Mustard-Gas Simulant by Nanosized Porphyrin-Based Metal−Organic Frameworks. *ACS Appl. Nano Mater.* **2019**, *2* (1), 465−469.
(61) Goswami, S.; Miller, C. E.; Logsdon, J. L.; Buru, C. T.; Wu, Y.-L.; Bowman, D. N.; Islamoglu, T.; Asiri, A. M.; Cramer, C. J.; Wasielewski, M. R.; et al. Atomistic Approach Toward Selective Photocatalytic Oxidation of a Mustard-Gas Simulant: A Case Study with Heavy-Chalcogen-Containing PCN-57 Analogues. *ACS Appl. Mater. Interfaces* **2017**, *9*, 19535−19540.
(62) Katz, M. J.; Mondloch, J. E.; Totten, R. K.; Park, J. K.; Nguyen, S. T.; Farha, O. K.; Hupp, J. T. Simple and Compelling Biomimetic Metal−Organic Framework Catalyst for the Degradation of Nerve Agent Simulants. *Angew. Chem., Int. Ed.* **2014**, *53*, 497−501.
(63) Lee, D. T.; Jamir, J. D.; Peterson, G. W.; Parsons, G. N. Water-Stable Chemical-Protective Textiles via Euhedral Surface-Oriented 2D Cu−TCPP Metal-Organic Frameworks. *Small* **2019**, *15*, 1805133.
(64) Lee, D. T.; Zhao, J.; Peterson, G. W.; Parsons, G. N. Catalytic "MOF-Cloth" Formed via Directed Supramolecular Assembly of UiO-66-NH2 Crystals on Atomic Layer Deposition-Coated Textiles for Rapid Degradation of Chemical Warfare Agent Simulants. *Chem. Mater.* **2017**, *29*, 4894−4903.
(65) Vu, A.-T.; Ho, K.; Lee, C.-H. Removal of Gaseous Sulfur and Phosphorus Compounds by Carbon-Coated Porous Magnesium Oxide Composites. *Chem. Eng. J.* **2016**, *283*, 1234−1243.
(66) Arcibar-Orozco, J. A.; Giannakoudakis, D. A.; Bandosz, T. J. Copper Hydroxyl Nitrate/Graphite Oxide Composite as Superoxidant for the Decomposition/Mineralization of Organophosphate-Based Chemical Warfare Agent Surrogate. *Adv. Mater. Interfaces* **2015**, *2*, 1500215.
(67) Hou, Y.; An, H.; Zhang, Y.; Hu, T.; Yang, W.; Chang, S. Rapid Destruction of Two Types of Chemical Warfare Agent Simulants by Hybrid Polyoxomolybdates Modified by Carboxylic Acid Ligands. *ACS Catal.* **2018**, *8*, 6062−6069.
(68) Liang, H.; Yao, A.; Jiao, X.; Li, C.; Chen, D. Fast and Sustained Degradation of Chemical Warfare Agent Simulants Using Flexible Self-Supported Metal−Organic Framework Filters. *ACS Appl. Mater. Interfaces* **2018**, *10*, 20396−20403.
(69) Tian, Y.; Plonka, A. M.; Ebrahim, A. M.; Palomino, R. M.; Senanayake, S. D.; Balboa, A.; Gordon, W. O.; Troya, D.; Musaev, D. G.; Morris, J. R.; Mitchell, M. B.; Collins-Wildman, D. L.; Hill, C. L.; Frenkel, A. I. A Correlated Multimodal Approach Reveals Key Details of Nerve-Agent Decomposition by Single Site Zr-Based Polyoxometalates. *J. Phys. Chem. Lett.* **2019**, *10*, 2295−2299.
(70) Stassen, I.; Bueken, B.; Reinsch, H.; Oudenhoven, J.; Wouters, D.; Hajek, J.; Van Speybroeck, V.; Stock, N.; Vereecken, P.; Van Schaijk, R.; et al. Towards Metal−Organic Framework Based Field Effect Chemical Sensors: UiO-66-NH 2 for Nerve Agent Detection. *Chem. Sci.* **2016**, *7*, 5827−5832.
(71) Plonka, A. M.; Wang, Q.; Gordon, W. O.; Balboa, A.; Troya, D.; Guo, W.; Sharp, C. H.; Senanayake, S. D.; Morris, J. R.; Hill, C. L.; Frenkel, A. I. In situ Probes of Capture and Decomposition of Chemical Warfare Agent Simulants by Zr-based Metal Organic Frameworks. *J. Am. Chem. Soc.* **2017**, *139*, 599−602.
(72) Pecharsky, V.; Zavalij, P. *Fundamentals of Powder Diffraction and Structural Characterization of Materials*; Springer, 2005.
(73) Billinge, S. J.; Kanatzidis, M. G. Beyond Crystallography: the Study of Disorder, Nanocrystallinity and Crystallographically Challenged Materials with Pair Distribution Functions. *Chem. Commun.* **2004**, 749−760.
(74) Platero-Prats, A. E.; Mavrandonakis, A.; Gallington, L. C.; Liu, Y.; Hupp, J. T.; Farha, O. K.; Cramer, C. J.; Chapman, K. W. Structural Transitions of the Metal-Oxide Nodes within Metal−Organic Frameworks: On the Local Structures of NU-1000 and UiO-66. *J. Am. Chem. Soc.* **2016**, *138*, 4178−4185.
(75) King, G.; Soliz, J. R.; Gordon, W. O. Local Structure of Zr(OH)4 and the Effect of Calcination Temperature from X-ray Pair Distribution Function Analysis. *Inorg. Chem.* **2018**, *57*, 2797−2803.
(76) Henderson, G. S.; de Groot, F. M. F.; Moulton, B. J. A. X-ray Absorption Near-Edge Structure (XANES) Spectroscopy. *Rev. Mineral. Geochem.* **2014**, *78*, 75−138.
(77) Timoshenko, J.; Duan, Z.; Henkelman, G.; Crooks, R. M.; Frenkel, A. I. Solving the Structure and Dynamics of Metal Nanoparticles by Combining X-Ray Absorption Fine Structure Spectroscopy and Atomistic Structure Simulations. *Annu. Rev. Anal. Chem.* **2019**, *12*, 501−522.
(78) Sayers, D. E.; Stern, E. A.; Lytle, F. W. New Technique for Investigating Noncrystalline Structures: Fourier Analysis of the Extended X-Ray Absorption Fine Structure. *Phys. Rev. Lett.* **1971**, *27*, 1204−1207.
(79) Rehr, J. J.; Albers, R. C. Theoretical approaches to X-ray Absorption Fine Structure. *Rev. Mod. Phys.* **2000**, *72*, 621−654.
(80) Lee, P. A.; Citrin, P. H.; Eisenberger, P.; Kincaid, B. M. Extended X-ray Absorption Fine Structure its Strengths and Limitations as a Structural Tool. *Rev. Mod. Phys.* **1981**, *53*, 769−806.
(81) Bare, S. R.; Mickelson, G. E.; Modica, F. S.; Ringwelski, A. Z.; Yang, N. Simple Flow Through Reaction Cells for In Situ Transmission and Fluorescence X-ray Absorption Spectroscopy of Heterogeneous Catalysts. *Rev. Sci. Instrum.* **2006**, *77*, 023105.

DOI: 10.1021/acsami.9b19494
ACS Appl. Mater. Interfaces 2020, 12, 14721−14738

(82) Li, Y.; Zakharov, D.; Zhao, S.; Tappero, R.; Jung, U.; Elsen, A.; Baumann, Ph.; Nuzzo, R. G.; Stach, E. A.; Frenkel, A. I. Complex Structural Dynamics of Nanocatalysts Revealed in *Operando* Conditions by Correlated Imaging and Spectroscopy Probes. *Nat. Commun.* **2015**, *6*, 7583.
(83) Swartz, W. E. X-ray Photoelectron Spectroscopy. *Anal. Chem.* **1973**, *45*, 788−800.
(84) Hollander, J. M.; Jolly, W. L. X-ray Photoelectron Spectroscopy. *Acc. Chem. Res.* **1970**, *3*, 193−200.
(85) Ginnard, C. R.; Riggs, W. M. X-ray Photoelectron Spectroscopy of Fluoropolymers. *Anal. Chem.* **1972**, *44*, 1310−1312.
(86) Ray, S.; Shard, A. G. Quantitative Analysis of Adsorbed Proteins by X-ray Photoelectron Spectroscopy. *Anal. Chem.* **2011**, *83*, 8659−8666.
(87) Dedryvère, R.; Maccario, M.; Croguennec, L.; Le Cras, F.; Delmas, C.; Gonbeau, D. X-Ray Photoelectron Spectroscopy Investigations of Carbon-Coated LixFePO4Materials. *Chem. Mater.* **2008**, *20*, 7164−7170.
(88) Petrovykh, D. Y.; Kimura-Suda, H.; Tarlov, M. J.; Whitman, L. J. Quantitative Characterization of DNA Films by X-ray Photoelectron Spectroscopy. *Langmuir* **2004**, *20*, 429−440.
(89) Taylor, A. Practical surface analysis. *Auger and X-ray Photoelectron Spectroscopy*, 2nd ed., Vol. *I*; Briggs, D., Seah, M. P., Eds.; John Wiley: New York, 1990; p 657.
(90) Stojilovic, N. Why Can't We See Hydrogen in X-ray Photoelectron Spectroscopy? *J. Chem. Educ.* **2012**, *89*, 1331−1332.
(91) Chen, D. A.; Ratliff, J. S.; Hu, X.; Gordon, W. O.; Senanayake, S. D.; Mullins, D. R. Dimethyl Methylphosphonate Decomposition on Fully Oxidized and Partially Reduced Ceria Thin Films. *Surf. Sci.* **2010**, *604*, 574−587.
(92) Head, A. R.; Tsyshevsky, R.; Trotochaud, L.; Eichhorn, B.; Kuklja, M. M.; Bluhm, H. Electron Spectroscopy and Computational Studies of Dimethyl Methylphosphonate. *J. Phys. Chem. A* **2016**, *120*, 1985−1991.
(93) Tudisco, C.; Betti, P.; Motta, A.; Pinalli, R.; Bombaci, L.; Dalcanale, E.; Condorelli, G. G. Cavitand-Functionalized Porous Silicon as an Active Surface for Organophosphorus Vapor Detection. *Langmuir* **2012**, *28*, 1782−1789.
(94) Head, A. R.; Tsyshevsky, R.; Trotochaud, L.; Yu, Y.; Kyhl, L.; Karslıoğlu, O.; Kuklja, M. M.; Bluhm, H. Adsorption of Dimethyl Methylphosphonate on MoO3: The Role of Oxygen Vacancies. *J. Phys. Chem. C* **2016**, *120*, 29077−29088.
(95) Trotochaud, L.; Head, A. R.; Büchner, C.; Yu, Y.; Karslıoğlu, O.; Tsyshevsky, R.; Holdren, S.; Eichhorn, B.; Kuklja, M. M.; Bluhm, H. Room temperature Decomposition of Dimethyl Methylphosphonate on Cuprous Oxide Yields Atomic Phosphorus. *Surf. Sci.* **2019**, *680*, 75−87.
(96) Kim, H.; Lee, B. S.; Lee, Y.; Lee, J. K.; Choi, I. S. Solid-phase Extraction of Nerve Agent Degradation Products Using poly[(2-(methacryloyloxy)ethyl)trimethylammonium chloride] Thin Films. *Talanta* **2019**, *197*, 500−508.
(97) Nieuwenhuizen, M. S.; Harteveld, J. L. N. Studies on a Surface Acoustic Wave (SAW) Dosimeter Sensor for Organophosphorous Nerve Agents. *Sens. Actuators, B* **1997**, *40*, 167−173.
(98) Ma, S.; Zhou, J.; Kang, Y. C.; Reddic, J. E.; Chen, D. A. Dimethyl Methylphosphonate Decomposition on Cu Surfaces: Supported Cu Nanoclusters and Films on TiO2(110). *Langmuir* **2004**, *20*, 9686−9694.
(99) Trotochaud, L.; Tsyshevsky, R.; Holdren, S.; Fears, K.; Head, A. R.; Yu, Y.; Karslıoğlu, O.; Pletincx, S.; Eichhorn, B.; Owrutsky, J.; Long, J.; Zachariah, M.; Kuklja, M. M.; Bluhm, H. Spectroscopic and Computational Investigation of Room-Temperature Decomposition of a Chemical Warfare Agent Simulant on Polycrystalline Cupric Oxide. *Chem. Mater.* **2017**, *29*, 7483−7496.
(100) Ratliff, J. S.; Tenney, S. A.; Hu, X.; Conner, S. F.; Ma, S.; Chen, D. A. Decomposition of Dimethyl Methylphosphonate on Pt, Au, and Au−Pt Clusters Supported on TiO2(110). *Langmuir* **2009**, *25*, 216−225.
(101) Jang, Y. J.; Kim, K.; Tsay, O. G.; Atwood, D. A.; Churchill, D. G. Update 1 of: Destruction and Detection of Chemical Warfare Agents. *Chem. Rev.* **2015**, *115*, PR1−PR76.
(102) Koskela, H. Use of NMR techniques for Toxic Organophosphorus Compound Profiling. *J. Chromatogr. B: Anal. Technol. Biomed. Life Sci.* **2010**, *878*, 1365−1381.
(103) Hiscock, J. R.; Sambrook, M. R.; Ede, J. A.; Wells, N. J.; Gale, P. A. Disruption of a Binary Organogel by the Chemical Warfare Agent Soman (GD) and Common Organophosphorus Simulants. *J. Mater. Chem. A* **2015**, *3*, 1230−1234.
(104) Mesilaakso, M.; Tolppa, E.-L. Detection of Trace Amounts of Chemical Warfare Agents and Related Compounds in Rubber, Paint, and Soil Samples by 1H and 31P{1H} NMR Spectroscopy. *Anal. Chem.* **1996**, *68*, 2313−2318.
(105) Koskela, H.; Grigoriu, N.; Vanninen, P. Screening and Identification of Organophosphorus Compounds Related to the Chemical Weapons Convention with 1D and 2D NMR Spectroscopy. *Anal. Chem.* **2006**, *78*, 3715−3722.
(106) de Koning, M. C.; van Grol, M.; Breijaert, T. Degradation of Paraoxon and the Chemical Warfare Agents VX, Tabun, and Soman by the Metal−Organic Frameworks UiO-66-NH2, MOF-808, NU-1000, and PCN-777. *Inorg. Chem.* **2017**, *56*, 11804−11809.
(107) Collins-Wildman, D. L.; Kim, M.; Sullivan, K. P.; Plonka, A. M.; Frenkel, A. I.; Musaev, D. G.; Hill, C. L. Buffer-Induced Acceleration and Inhibition in Polyoxometalate-Catalyzed Organophosphorus Ester Hydrolysis. *ACS Catal.* **2018**, *8*, 7068−7076.
(108) Luong, T. K. N.; Shestakova, P.; Absillis, G.; Parac-Vogt, T. N. Detailed Mechanism of Phosphoanhydride Bond Hydrolysis Promoted by a Binuclear ZrIV-Substituted Keggin Polyoxometalate Elucidated by a Combination of 31P, 31P DOSY, and 31P EXSY NMR Spectroscopy. *Inorg. Chem.* **2016**, *55*, 4864−4873.
(109) Brevett, C. A. S.; Sumpter, K. B. Degradation of the chemical warfare agents HD, GD, Thickened GD, and VX on Ambient and Moist Environmental Substrates. *Main Group Chem.* **2010**, *9*, 205−219.
(110) Grassian, V. H.; Larsen, S. C. Applications of Nanocrystalline Zeolites to CWA Decontamination. *Nanoscience and Nanotechnology for Chemical and Biological Defense*; American Chemical Society, 2009; Vol. *1016*, pp 249−260.
(111) Columbus, I.; Waysbort, D.; Marcovitch, I.; Yehezkel, L.; Mizrahi, D. M. VX Fate on Common Matrices: Evaporation versus Degradation. *Environ. Sci. Technol.* **2012**, *46*, 3921−3927.
(112) Jain, M. G.; Mote, K. R.; Hellwagner, J.; Rajalakshmi, G.; Ernst, M.; Madhu, P. K.; Agarwal, V. Measuring Strong One-bond Dipolar Couplings using REDOR in Magic-Angle Spinning Solid-State NMR. *J. Chem. Phys.* **2019**, *150*, 134201.
(113) Polenova, T.; Gupta, R.; Goldbourt, A. Magic Angle Spinning NMR Spectroscopy: A Versatile Technique for Structural and Dynamic Analysis of Solid-Phase Systems. *Anal. Chem.* **2015**, *87*, 5458−5469.
(114) Kirkpatrick, R. J.; Dunn, T.; Schramm, S.; Smith, K. A.; Oestrike, R.; Turner, G. Magic-Angle Sample-Spinning Nuclear Magnetic Resonance Spectroscopy of Silicate Glasses: A Review. *Structure and Bonding in Noncrystalline Solids*; Walrafen, G. E., Revesz, A. G., Eds.; Springer US: Boston, MA, 1986; pp 303−327.
(115) Mondloch, J. E.; Katz, M. J.; Isley, W. C., III; Ghosh, P.; Liao, P.; Bury, W.; Wagner, G. W.; Hall, M. G.; DeCoste, J. B.; Peterson, G. W.; Snurr, R. Q.; Cramer, C. J.; Hupp, J. T.; Farha, O. K. Destruction of Chemical Warfare Agents Using Metal−Organic Frameworks. *Nat. Mater.* **2015**, *14*, 512−516.
(116) Wagner, G. W.; Koper, O. B.; Lucas, E.; Decker, S.; Klabunde, K. J. Reactions of VX, GD, and HD with Nanosize CaO: Autocatalytic Dehydrohalogenation of HD. *J. Phys. Chem. B* **2000**, *104*, 5118−5123.
(117) Wagner, G. W.; Bartram, P. W.; Koper, O.; Klabunde, K. J. Reactions of VX, GD, and HD with Nanosize MgO. *J. Phys. Chem. B* **1999**, *103*, 3225−3228.
(118) Wagner, G. W.; Procell, L. R.; O'Connor, R. J.; Munavalli, S.; Carnes, C. L.; Kapoor, P. N.; Klabunde, K. J. Reactions of VX, GB,

DOI: 10.1021/acsami.9b19494
ACS Appl. Mater. Interfaces 2020, 12, 14721−14738

GD, and HD with Nanosize Al2O3. Formation of Aluminophosphonates. *J. Am. Chem. Soc.* **2001**, *123*, 1636−1644.
(119) Wagner, G. W.; Chen, Q.; Wu, Y. Reactions of VX, GD, and HD with Nanotubular Titania. *J. Phys. Chem. C* **2008**, *112*, 11901−11906.
(120) Wagner, G. W.; Peterson, G. W.; Mahle, J. J. Effect of Adsorbed Water and Surface Hydroxyls on the Hydrolysis of VX, GD, and HD on Titania Materials: The Development of Self-Decontaminating Paints. *Ind. Eng. Chem. Res.* **2012**, *51*, 3598−3603.
(121) Bandosz, T. J.; Laskoski, M.; Mahle, J.; Mogilevsky, G.; Peterson, G. W.; Rossin, J. A.; Wagner, G. W. Reactions of VX, GD, and HD with Zr(OH)4: Near Instantaneous Decontamination of VX. *J. Phys. Chem. C* **2012**, *116*, 11606−11614.
(122) Peterson, G. W.; Wagner, G. W. Detoxification of chemical warfare agents by CuBTC. *J. Porous Mater.* **2014**, *21*, 121−126.
(123) Peterson, G. W.; Moon, S.-Y.; Wagner, G. W.; Hall, M. G.; DeCoste, J. B.; Hupp, J. T.; Farha, O. K. Tailoring the Pore Size and Functionality of UiO-Type Metal−Organic Frameworks for Optimal Nerve Agent Destruction. *Inorg. Chem.* **2015**, *54*, 9684−9686.
(124) Wagner, G. W.; MacIver, B. K.; Yang, Y.-C. Magic Angle Spinning NMR Study of Adsorbate Reactions on Activated Charcoal. *Langmuir* **1995**, *11*, 1439−1442.
(125) Saalwächter, K. Chapter 1 Applications of NMR in Polymer Characterization—An Introduction. In *NMR Methods for Characterization of Synthetic and Natural Polymers*; Royal Soc. Chem., 2019; pp 1−22.
(126) Mafra, L.; Vidal-Moya, J. A.; Blasco, T., Chapter Four—Structural Characterization of Zeolites by Advanced Solid State NMR Spectroscopic Methods. *Annual Reports NMR Spectroscpy*; Webb, G. A., Ed.; Academic Press, 2012; Vol. *77*, pp 259−351.
(127) Keeler, C.; Maciel, G. E. Quantitation in the Solid-State ^{13}C NMR Analysis of Soil and Organic Soil Fractions. *Anal. Chem.* **2003**, *75*, 2421−2432.
(128) Walkley, B.; Provis, J. L. Solid-state Nuclear Magnetic Resonance Spectroscopy of Cements. *Mater. Today Adv.* **2019**, *1*, 100007.
(129) Hilbig, H.; Köhler, F. H.; Schießl, P. Quantitative ^{29}Si MAS NMR Spectroscopy of Cement and Silica Fume Containing Paramagnetic Impurities. *Cem. Concr. Res.* **2006**, *36*, 326−329.
(130) Zafrani, Y.; Goldvaser, M.; Dagan, S.; Feldberg, L.; Mizrahi, D.; Waysbort, D.; Gershonov, E.; Columbus, I. Degradation of Sulfur Mustard on KF/Al_2O_3 Supports: Insights into the Products and the Reactions Mechanisms. *J. Org. Chem.* **2009**, *74*, 8464−8467.
(131) Gershonov, E.; Columbus, I.; Zafrani, Y. Facile Hydrolysis-Based Chemical Destruction of the Warfare Agents VX, GB, and HD by Alumina-Supported Fluoride Reagents. *J. Org. Chem.* **2009**, *74*, 329−338.
(132) Fridkin, G.; Yehezkel, L.; Columbus, I.; Zafrani, Y. Solvent Effects on the Reactions of the Nerve Agent VX with KF/Al_2O_3: Heterogeneous or Homogeneous Decontamination? *J. Org. Chem.* **2016**, *81*, 2154−2158.
(133) Chen, P. C.; Joyner, C. C.; Patrick, S. T.; Benton, K. F. High-Speed High-Resolution Gas-Phase Raman Spectroscopy. *Anal. Chem.* **2002**, *74*, 1618−1623.
(134) Merlin, R.; Pinczuk, A.; Weber, W. H. Overview of Phonon Raman Scattering in Solids. *Raman Scattering in Materials Science*; Weber, W. H., Merlin, R., Eds.; Springer: Berlin, 2000; pp 1−29.
(135) Bumbrah, G. S.; Sharma, R. M. Raman spectroscopy − Basic Principle, Instrumentation and Selected Applications for the Characterization of Drugs of Abuse. *Egy. J. Forensic Sci.* **2016**, *6*, 209−215.
(136) Devine, T. M.; Adar, F. Raman Spectroscopy of Solids. *Optical Imaging and Spectroscopy*; Wiley Online Library, 2012; pp 1−38.
(137) Mulvaney, S. P.; Keating, C. D. Raman Spectroscopy. *Anal. Chem.* **2000**, *72*, 145−158.
(138) Lyon, L. A.; Keating, C. D.; Fox, A. P.; Baker, B. E.; He, L.; Nicewarner, S. R.; Mulvaney, S. P.; Natan, M. J. Raman Spectroscopy. *Anal. Chem.* **1998**, *70*, 341−362.
(139) Costa, J. C. S.; Ando, R. A.; Camargo, P. H. C.; Corio, P. Understanding the Effect of Adsorption Geometry over Substrate Selectivity in the Surface-Enhanced Raman Scattering Spectra of Simazine and Atrazine. *J. Phys. Chem. C* **2011**, *115*, 4184−4190.
(140) Wei, W.; Du, Y.; Zhang, L.; Yang, Y.; Gao, Y. Improving SERS Hot Spots for On-site Pesticide Detection by Combining Silver Nanoparticles with Nanowires. *J. Mater. Chem. C* **2018**, *6*, 8793−8803.
(141) Wang, Y.; Alsmeyer, D. C.; McCreery, R. L. Raman Spectroscopy of Carbon Materials: Structural Basis of Observed Spectra. *Chem. Mater.* **1990**, *2*, 557−563.
(142) Lazarević-Pašti, T.; Anićijević, V.; Baljozović, M.; Anićijević, D. V.; Gutić, S.; Vasić, V.; Skorodumova, N. V.; Pašti, I. A. The Impact of the Structure of Graphene-based Materials on the Removal of Organophosphorus Pesticides from Water. *Environ. Sci.: Nano* **2018**, *5*, 1482−1494.
(143) Wachs, I. E. Raman and IR Studies of Surface Metal Oxide Species on Oxide Supports: Supported Metal Oxide Catalysts. *Catal. Today* **1996**, *27*, 437−455.
(144) Ekoi, E. J.; Gowen, A.; Dorrepaal, R.; Dowling, D. P. Characterisation of titanium oxide layers using Raman spectroscopy and optical profilometry: Influence of oxide properties. *Results Phys.* **2019**, *12*, 1574−1585.
(145) Samuel, A. Z.; Zhou, M.; Ando, M.; Mueller, R.; Liebert, T.; Heinze, T.; Hamaguchi, H.-o. Determination of Percent Crystallinity of Side-Chain Crystallized Alkylated-Dextran Derivatives with Raman Spectroscopy and Multivariate Curve Resolution. *Anal. Chem.* **2016**, *88*, 4644−4650.
(146) Conti, C.; Realini, M.; Colombo, C.; Sowoidnich, K.; Afseth, N. K.; Bertasa, M.; Botteon, A.; Matousek, P. Noninvasive Analysis of Thin Turbid Layers Using Microscale Spatially Offset Raman Spectroscopy. *Anal. Chem.* **2015**, *87*, 5810−5815.
(147) Gerrard, D. L. Raman Spectroscopy. *Anal. Chem.* **1994**, *66*, 547−557.
(148) Durig, J. R.; Cox, A. W. Spectra and structure of organophosphorus compounds. 16. Infrared and Raman Spectra, Vibrational Assignment, and Conformational Analysis for isopropylphosphine and isopropylphosphine-d2. *J. Phys. Chem.* **1976**, *80*, 2493−2498.
(149) Bowen, J. M.; Powers, C. R.; Ratcliffe, A. E.; Rockley, M. G.; Hounslow, A. W. Fourier Transform Infrared and Raman Spectra of Dimethyl Methylphosphonate Adsorbed on Montmorillonite. *Environ. Sci. Technol.* **1988**, *22*, 1178−1181.
(150) Mäkie, P.; Westin, G.; Persson, P.; Österlund, L. Adsorption of Trimethyl Phosphate on Maghemite, Hematite, and Goethite Nanoparticles. *J. Phys. Chem. A* **2011**, *115*, 8948−8959.
(151) Majumdar, D.; Roszak, S.; Leszczynski, J. Density Functional Theory Based Studies on the Nature of Raman and Resonance Raman Scattering of Nerve Agent Bound to Gold and Oxide-Supported Gold Clusters: A Plausible Way of Detection. *J. Phys. Chem. A* **2010**, *114*, 4340−4353.
(152) Taranenko, N.; Alarie, J.-P.; Stokes, D. L.; Vo-Dinh, T. Surface-Enhanced Raman Detection of Nerve Agent Simulant (DMMP and DIMP) Vapor on Electrochemically Prepared Silver Oxide Substrates. *J. Raman Spectrosc.* **1996**, *27*, 379−384.
(153) Kondo, T.; Hashimoto, R.; Ohrui, Y.; Sekioka, R.; Nogami, T.; Muta, F.; Seto, Y. Analysis of Chemical Warfare Agents by Portable Raman Spectrometer with both 785nm and 1064nm Excitation. *Forensic Sci. Int.* **2018**, *291*, 23−38.
(154) Hu, G.; Xiong, W.; Luo, H.; Shi, H.; Li, Z.; Shen, J.; Fang, X.; Xu, B.; Zhang, J. Raman Spectroscopic Detection for Simulants of Chemical Warfare Agents Using a Spatial Heterodyne Spectrometer. *Appl. Spectrosc.* **2018**, *72*, 151−158.
(155) Choi, S.-K.; Jeong, Y.-S.; Koh, Y. J.; Lee, J. H.; Nam, H.-W.; Lee, J. Analysis of Raman Spectral Characteristics of Chemical Warfare Agents by Using 248-nm UV Raman Spectroscopy. *Bull. Korean Chem. Soc.* **2019**, *40*, 279−284.

DOI: 10.1021/acsami.9b19494
ACS Appl. Mater. Interfaces 2020, 12, 14721−14738

(156) McKelvy, M. L.; Britt, T. R.; Davis, B. L.; Gillie, J. K.; Lentz, L. A.; Leugers, A.; Nyquist, R. A.; Putzig, C. L. Infrared Spectroscopy. *Anal. Chem.* **1996**, *68*, 93−160.
(157) Bergaya, F.; Gates, W. P.; Madejová, J.; Kloprogge, J. T.; Bain, D., Chapter 1—General Introduction. In *Developments in Clay Science*; Gates, W. P., Kloprogge, J. T., Madejová, J., Bergaya, F., Eds.; Elsevier, 2017; Vol. *8*, pp 1−5.
(158) Maréchal, Y. 4—Infrared and Related Spectroscopies of H-Bonded Systems: Experimental Point of View. In *The Hydrogen Bond and the Water Molecule*; Maréchal, Y., Ed.; Elsevier: Amsterdam, 2007; pp 77−113.
(159) Hair, M. L. Transmission Infrared Spectroscopy for High Surface Area Oxides. In *Vibrational Spectroscopies for Adsorbed Species*; American Chemical Society, 1980; Vol. *137*, pp 1−11.
(160) Colón-Ortiz, J.; Landers, J. M.; Gordon, W. O.; Balboa, A.; Karwacki, C. J.; Neimark, A. V. Disordered Mesoporous Zirconium (Hydr)oxides for Decomposition of Dimethyl Chlorophosphate. *ACS Appl. Mater. Interfaces* **2019**, *11*, 17931−17939.
(161) Gordon, W. O.; Tissue, B. M.; Morris, J. R. Adsorption and Decomposition of Dimethyl Methylphosphonate on Y_2O_3 Nanoparticles. *J. Phys. Chem. C* **2007**, *111*, 3233−3240.
(162) Ferguson-McPherson, M. K.; Low, E. R.; Esker, A. R.; Morris, J. R. Corner Capping of Silsesquioxane Cages by Chemical Warfare Agent Simulants. *Langmuir* **2005**, *21*, 11226−11231.
(163) Wilmsmeyer, A. R.; Gordon, W. O.; Davis, E. D.; Troya, D.; Mantooth, B. A.; Lalain, T. A.; Morris, J. R. Infrared Spectra and Binding Energies of Chemical Warfare Nerve Agent Simulants on the Surface of Amorphous Silica. *J. Phys. Chem. C* **2013**, *117*, 15685−15697.
(164) Moss, J. A.; Szczepankiewicz, S. H.; Park, E.; Hoffmann, M. R. Adsorption and Photodegradation of Dimethyl Methylphosphonate Vapor at TiO_2 Surfaces. *J. Phys. Chem. B* **2005**, *109*, 19779−19785.
(165) Panayotov, D. A.; Morris, J. R. Thermal Decomposition of a Chemical Warfare Agent Simulant (DMMP) on TiO_2: Adsorbate Reactions with Lattice Oxygen as Studied by Infrared Spectroscopy. *J. Phys. Chem. C* **2009**, *113* (35), 15684−15691.
(166) Chapleski, R. C.; Musaev, D. G.; Hill, C. L.; Troya, D. Reaction Mechanism of Nerve-Agent Hydrolysis with the $Cs_8Nb_6O_{19}$ Lindqvist Hexaniobate Catalyst. *J. Phys. Chem. C* **2016**, *120*, 16822−16830.
(167) Odoh, S. O.; Cramer, C. J.; Truhlar, D. G.; Gagliardi, L. Quantum-Chemical Characterization of the Properties and Reactivities of Metal−Organic Frameworks. *Chem. Rev.* **2015**, *115*, 6051−6111.
(168) Momeni, M. R.; Cramer, C. J. Computational Screening of Roles of Defects and Metal Substitution on Reactivity of Different Single- vs Double-Node Metal−Organic Frameworks for Sarin Decomposition. *J. Phys. Chem. C* **2019**, *123*, 15157−15165.
(169) Momeni, M. R.; Cramer, C. J. Dual Role of Water in Heterogeneous Catalytic Hydrolysis of Sarin by Zirconium-Based Metal-Organic Frameworks. *ACS Appl. Mater. Interfaces* **2018**, *10*, 18435−18439.
(170) Chen, H.; Liao, P.; Mendonca, M. L.; Snurr, R. Q. Insights into Catalytic Hydrolysis of Organophosphate Warfare Agents by Metal−Organic Framework NU-1000. *J. Phys. Chem. C* **2018**, *122*, 12362−12368.
(171) Wang, G.; Sharp, C.; Plonka, A. M.; Wang, Q.; Frenkel, A. I.; Guo, W.; Hill, C. L.; Smith, C.; Kollar, J.; Troya, D.; Morris, J. R. Mechanism and Kinetics for Reaction of the Chemical Warfare Agent Simulant, DMMP(g), with Zirconium(IV) MOFs: An Ultrahigh-Vacuum and DFT Study. *J. Phys. Chem. C* **2017**, *121*, 11261−11272.
(172) Plonka, A. M.; Grissom, T. G.; Musaev, D. G.; Balboa, A.; Gordon, W. O.; Collins-Wildman, D. L.; Ghose, S. K.; Tian, Y.; Ebrahim, A. M.; Mitchell, M. B.; Hill, C. L.; Morris, J. R.; Frenkel, A. I. Effect of Carbon Dioxide on the Degradation of Chemical Warfare Agent Simulant in the Presence of Zr Metal Organic Framework MOF-808. *Chem. Mater.* **2019**, *31*, 9904.

DOI: 10.1021/acsami.9b19494
ACS Appl. Mater. Interfaces 2020, 12, 14721−14738